Processing of Piezoelectric Silk Films and Examination of Stability of Piezoelectric Effect

A thesis

submitted by

Kathleen Martinick

In partial fulfillment of the requirements

for the degree of

Masters of Science

In

Bioengineering

TUFTS UNIVERSITY

August 2012

Advisor: Professor David Kaplan, Ph. D.

Committee member: Professor Fiorenzo Omenetto, Ph. D.

Cross department committee member: Professor Peggy Cebe, Ph. D.

Abstract

Finding biocompatible and biodegradable substrates for biomedical engineering applications continues to be a major focus today. *Bombyx mori* silk has received attention as a useful biopolymer for its remarkable mechanical properties, biocompatibility and the high level of control over degradation rates; moreover, the degradation products are amino acids the body can reuse. It has been found that native silk fibers display piezoelectricity rivaling that of quartz, and more recently the piezoelectric effect has been recreated in regenerated silk fibroin films. A zone drawing technique has been used to induce β-sheet alignment as well as increase β-sheet content, key components to piezoelectric silk films. A modified dynamic mechanical analyzer was used to measure current and voltage under applied stress, and piezoelectric strain and voltage constants were calculated. Performance of films treated to induce water insolubility has been examined to find optimal processing parameters. Stability of water insoluble films has been investigated. By altering post treatments, it is possible to improve piezoelectric strain constants and maintain piezoelectricity for more than 130, 000 cycles. The successful demonstration of piezoelectric films made from biological polymers offers exciting ideas for future biomedical tissue engineering and sensing applications.

Acknowledgements

I would like to thank my committee members, David Kaplan, Peggy Cebe, and Fiorenzo Omenetto for their guidance over the course of the last two years. I am especially grateful to David Kaplan for the opportunity to pursue this exciting research. I am incredibly thankful for the opportunity to work on collaborative projects and learn about research areas outside my own.

I would like to thank Thomas Scheibel, Stefanie Wohlrab, and the rest of Scheibel lab at the University of Bayreuth for the opportunity to work on the spider silk collaboration. I also want to thank them for their incredible hospitality during my visit.

I would like to thank my colleagues at Tufts, especially Tuna Yucel, Xiao Hu, and Danielle Rockwood for helping me get started in the labs and providing added guidance over the course of my research. I would also like to thank Wenwen Huang and Sreevidhya Tarakkad Krishnaji for teaching me new methodologies. I would like to thank the Silk Processing and Chemistry group for their continual feedback and suggestions, especially Kelly Burke, Waseem Raja, and Yinan Lin. Finally, I would like to thank the Kaplan lab in its entirety for making the past two years enjoyable and productive.

Lastly, I would like to thank my family and friends for their incredible support during my research. To my parents who have been amazing cheerleaders and constantly told me to go outside, that lab work can wait. I would like to thank my siblings, who provided the perfect distractions some days. I would like to thank my friends both at Tufts and elsewhere for providing constant laughter, and keeping me motivated with the always innocent question “Aren’t you done with school *yet*?”

Contents

List of Tables

List of Figures

Introduction

Fundamental Aspects of Piezoelectricity

The piezoelectric effect describes the phenomenon whereby an electrical polarization occurs as a result of an applied force (Martin, 1972; Kepler and Anderson, 1980). Moreover, the magnitude of polarization is proportional to the magnitude of the applied force. The phenomenon operates in the opposite direction as well; an applied potential difference will result in mechanical strain. On the molecular level, this process is the result of many dipole moments within a material aligning in response to the applied force, which can be observed in the form of current flow or a potential drop across the material (**Figure 1,** Kepler and Anderson, 1980).

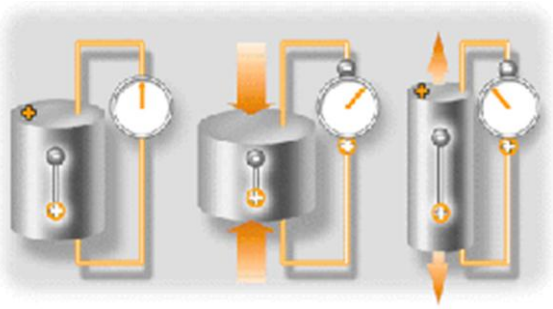

Figure 1: Basic Piezoelectric effect. *Left*: A piezoelectric material in the absence of any applied force. Notice the voltmeter reads zero. *Center*: A generated voltage under compressive stress. *Right*: A generated voltage under tensile stress. Here, the voltmeter reads opposite polarity between the compressive and tensile force. (Image from http://www.topbits.com/piezoelectric-effect.html)

In order for such an effect to be observed, a material must meet several criteria. First, a dipole moment must exist within the crystal unit of the material. In an amorphous polymer, the dipole moments must be aligned and locked in that orientation (Ounaies *et al.*, 1999). This is the basis of the observed polarization. Secondly, the crystal unit must possess an axis of asymmetry that allows for the

manipulation of the dipole moment. Without the asymmetry, a crystalline unit will cancel the effect of neighboring dipole moments. Finally, the crystalline units must be aligned in order to allow for an observable effect; randomly aligned units will result in only a fraction of the total sample responding to an applied force and likely results in negligible piezoelectric properties. Taken together, the observed piezoelectric effect results from contributions of each element in the following relationship:

$$d_{14} = \phi F_c (d_{14}^c - d_{25}^c)/2 \quad (1)$$

Where ϕ is the degree of crystallinity, F_c is the degree of orientation of the crystalline units, the d values are piezoelectric constant values indicating how much charge is generated per force applied (described in detail below). The c superscript denotes the value for a single crystal (Furukawa, 1989).

In order to directly compare the properties of different piezoelectric materials, constants have been defined to normalize electrical output to mechanical input (Furukawa, 1989). **Figure 2** shows the different ways the inputs and outputs can be related to each other. For the purposes of this work, the direct piezoelectric effect was studied by applying stress, so the two equations of interest are:

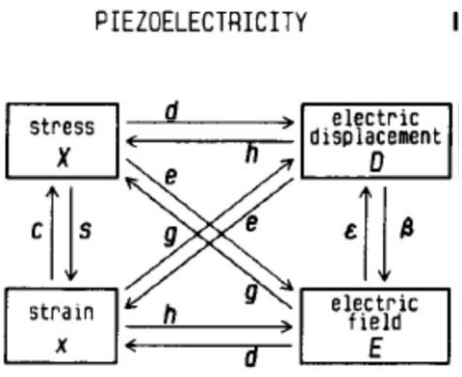

Figure 2: Relationships between mechanical and electrical properties of piezoelectric response (Furukawa, 1989)

$$D_i = d_{ij} X_j \quad (2)$$

$$E_i = -g_{ij} X_j \quad (3)$$

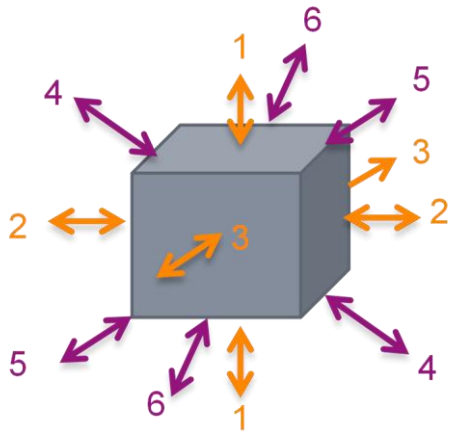

Figure 3: Planes corresponding to numbered force and polarization tensors. Normal forces are solid gold, and shear forces are purple.

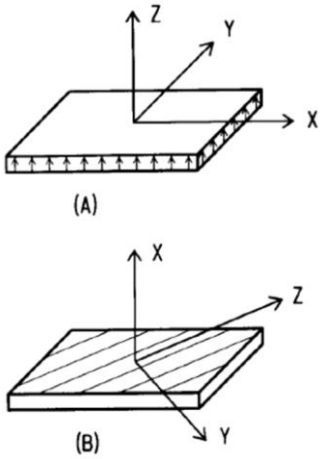

Figure 4: Resulting molecular alignment in polymer films after (A) DC field alignment and (B) mechanical alignment (Furukawa, 1989).

These equations can be seen in **Figure 2**. In **Equation 2**, D is the electrical depolarization, d is the piezoelectric strain constant, and X is the applied stress. The subscripts are defined below. Similarly in **Equation 3**, E is the electric field generated under applied stress X, and g is the piezoelectric voltage constant.

The subscripts i and j denote the direction of the electrical property and the direction of applied force, respectively. The subscript i can take on a value from 1 to 3, while j can be a value from 1 to 6 (Fukada, 1995). Note that the values 1 through 3 refer to the same directions for both electrical and mechanical subscripts. These numbers correspond to different directional planes in a sample (**Figure 3**). By imparting a Cartesian coordinate system on a sample, the x, y, and z axes correspond to 1, 2, and 3, respectively. Values 4, 5, and 6 refer to the additional three shear force directions that may also be

applied to generate electricity. By convention, the z axis (or 3 direction) is always assigned to run parallel to the direction of molecular alignment within the given material (**Figure 4,** Furukawa, 1989).

Taking the possible combinations of input and output directions into consideration, matrix forms of **Equations 2 and 3** arise, as seen in **Equations 4** and **5**

$$\begin{bmatrix} P_1 \\ P_2 \\ P_3 \end{bmatrix} = \begin{bmatrix} d_{11} & d_{12} & d_{13} & d_{14} & d_{15} & d_{16} \\ d_{21} & d_{22} & d_{23} & d_{24} & d_{25} & d_{26} \\ d_{31} & d_{32} & d_{33} & d_{34} & d_{35} & d_{36} \end{bmatrix} \begin{bmatrix} X_1 \\ X_2 \\ X_3 \\ X_4 \\ X_5 \\ X_6 \end{bmatrix} \quad (4)$$

$$\begin{bmatrix} E_1 \\ E_2 \\ E_3 \end{bmatrix} = \begin{bmatrix} g_{11} & g_{12} & g_{13} & g_{14} & g_{15} & g_{16} \\ g_{21} & g_{22} & g_{23} & g_{24} & g_{25} & g_{26} \\ g_{31} & g_{32} & g_{33} & g_{34} & g_{35} & g_{36} \end{bmatrix} \begin{bmatrix} X_1 \\ X_2 \\ X_3 \\ X_4 \\ X_5 \\ X_6 \end{bmatrix} \quad (5)$$

In reality a material may not have a value at each element. Again, a material must possess an asymmetry in order for piezoelectricity to be possible. Any symmetry within a material results in different elements of the constant matrix turning to zero, leaving only a few nonzero elements in the matrix.

Piezoelectric Materials

Piezoelectricity has traditionally been found in materials with a highly uniform, highly crystalline, repeating structure. The majority of piezoelectric materials characterized and used in applications today are ceramic. Quartz is typically considered the "traditional" piezoelectric material, which is made of O—Si—O crystalline units (Martin, 1972; Jaffe 1958). Lead-Zirconate-Titanate (PZT) is also well-known as

the basis for ultrasound imaging technology. A number of different ceramic composites have also been made, and a comparison of their piezoelectric strain constant can be seen in **Table 1**.

Piezoelectric Constants of Common Piezoelectric Materials	
Material	**d_{ij} constant (pC/N)**
Ceramics: ij = 33	
Quartz[1]	2.3
$BaTiO_3$[1]	190
PZT-4 (Clevite Corp.)[1]	250
Synthetic Polymers: ij =31	
Polyvinylidene fluoride[2]	21
Polyvinyl chloride[2]	10
Polycarbonate[2]	0.5
Nylon 11[2]	0.5
Synthetic Polymers: ij = 25	
Poly-Ɣ-methyl-L-glutamate[2]	0.5
Poly-Ɣ-methyl-D-glutamate[2]	-1.3
Poly-Ɣ-benzyl-L-glutamate[2]	4
Poly-Ɣ-ethyl-D-glutamate[2]	-0.6
Poly-L-lactic acid[3]	10
Native Biopolymers: ij=14	
Cellulose –wood[3]	0.1
Chitin—lobster apodeme (demineralized) [3]	1.5
Silk fiber[3]	1
Amylose—starch[3]	2
Collagen—bone[3]	0.2
Collagen—tendon[3]	2
Keratin—horn[3]	1.8
Fibrin—elongated films of fibrinogen-thrombin clot[3]	0.2

Table 1: Piezoelectric strain constant of various materials. Appropriate subscripts for the constant are listed in the subheadings. [1]=Jaffe, 1958, [2]=Fukada, 1974, [3]=Fukada, 1995.

More recently, it has been found that native biological polymers inherently exhibit piezoelectricity. Samples from both bone and tendon display remarkable piezoelectric properties, their piezoelectric strain constants rivaling that of quartz (Bassett, 1972; Marino *et al.* 1980; Fukada, 1964**, Table 1**). Silk and keratin have been found to exhibit piezoelectricity as well (Fukada, 1995; Yucel *et al.*, 2011). Structural analysis of piezoelectric biopolymer samples revealed highly aligned structures. When

isolating the protein and trying to observe the piezoelectric effect in reconstituted forms, however, the alignment is not conserved, and the effect is severely reduced and almost vanishes (Silva et al, Marino *et al.*, 1980).

Inducing Piezoelectricity

For a given material, the presence of a dipole moment and any lattice asymmetry cannot be altered without changing the material itself. However, methods exist to induce alignment of molecules, and in particular polymers in films (Furukawa 1989). In general, polymers randomly align when cast into a film, which results in little or no observed piezoelectric effect. However, by inducing alignment, it is possible to drastically increase piezoelectric properties.

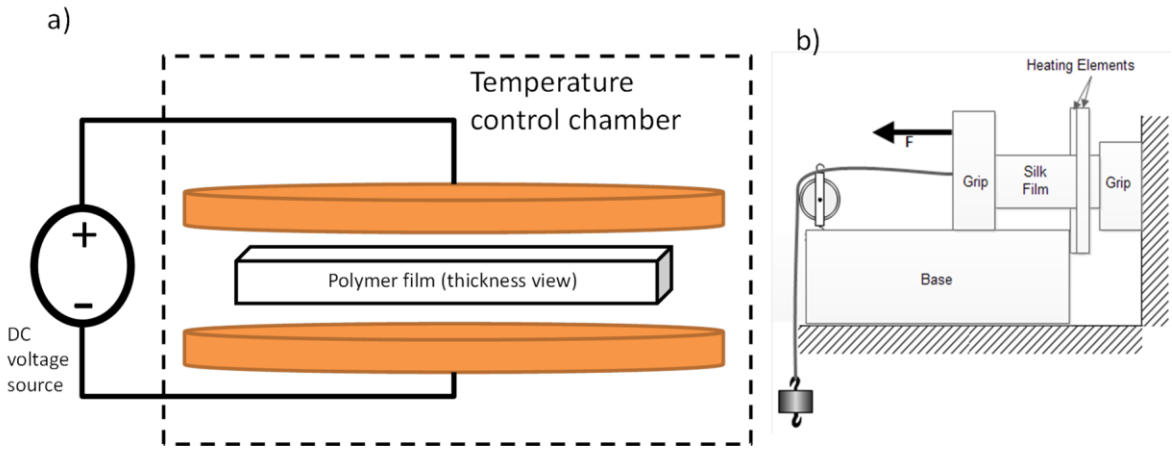

Figure 5: a) Schematic of alignment method using electric fields to create class C piezoelectricity. B) Alignment method using mechanical force to create class D polymers.

Two common methods exist to induce alignment in polymer films (**Figure 5)**. Both methods introduce added molecular mobility in the form of thermal energy to allow for rearrangement of structures without melting the film. The first method uses a large direct current (DC) electric field to

induce alignment along the field. Here, films are heated to the glass transition temperature, at which point the field is applied. With the electric field still applied, the film temperature is then reduced back to room temperature, effectively trapping the orientation of the polymers. This method yields materials characterized as "class C" polymers, and the d matrix in **Equation 4** becomes (Fukada, 1983):

$$d = \begin{bmatrix} 0 & 0 & 0 & 0/d_{14} & d_{25} & 0 \\ 0 & 0 & 0 & d_{15} & 0/-d_{14} & 0 \\ d_{31} & d_{32} & d_{33} & 0 & 0 & 0 \end{bmatrix} \quad (6)$$

Depending on the molecular structure, shear piezoelectricity may or may not be present. If no shear piezoelectricity exists, d_{14} and d_{25} drop to zero; otherwise they are nonzero.

The second method uses mechanical force rather than electrical force to induce molecular alignment. Thermal energy is again used to provide mobility. With the film at the glass transition temperature, tension is applied to the film, causing alignment along the direction of the force. Films that have been drawn display shear piezoelectricity (Fukada, 1983).

$$d = \begin{bmatrix} 0 & 0 & 0 & d_{14} & 0 & 0 \\ 0 & 0 & 0 & 0 & -d_{14} & 0 \\ 0 & 0 & 0 & 0 & 0 & 0 \end{bmatrix} \quad (7)$$

The basis of the piezoelectric effect differs depending on the alignment method chosen and the polymer itself (Kepler and Anderson, 2006). The films can either display stress-induced piezoelectricity or permanent polarization. Stress-induced piezoelectricity describes the phenomena whereby films polarize only under applied stress; biological polymers and some oriented synthetic polymers fall into this category. Permanent polarization is much more common and is typically the result of poling films

with a large electric field. These films, called electrets, have essentially permanent polarizations because the orientation of the dipole has been frozen in place. The frozen in alignment, however, is not entirely stable.

Alignment methods have successfully been applied to synthetic polymer films to induce piezoelectricity. The most successful demonstration of piezoelectricity in polymers is that of PVDF. By aligning the polymer chains through mechanical stretching, the piezoelectric effect is increased. The magnitude can be even further exaggerated by aligning the CF_2 dipoles in an electric field after alignment (Fukada, 1974). Improved polarization of PVDF and copolymers containing PVDF has led these polymers to become the only piezoelectric polymers currently commercially available (Atkinson *et al.*, 2003).

In addition to PVDF, optically active synthetic polymers have received attention for piezoelectricity (**Table 1**). Since the optical activity of the polymers confirms right or left handed symmetry, and therefore asymmetry, these polymers have been rolled and stretched to exhibit piezoelectricity. By doing so, it has been possible to create a piezoelectric effect on the same order of magnitude as quartz. It is worth noting that the observed piezoelectric effect of L and D chiral polymers are opposite in sign.

Despite the promise such synthetic polymer films possess, their use in biomedical applications is limited by their unfavorable biocompatibility and undesirable degradation products (Gunatillake and Adhikari, 2003). Biopolymers offer improved biocompatibility, but little research has been completed to recreate the piezoelectric effect in isolated proteins (Yucel *et al*, 2011; Yang *et al*, 2006; Silva *et al.*, 2001; Marino *et al.*, 1980).

Silk

Silk derived from the *Bombyx mori* silkworm possesses material properties desirable for biomedical applications. In fact, silk fibers have been used as sutures for centuries (Altman *et al*, 2003). Silk fibers display remarkable mechanical properties, most noticeably toughness (Vendrely and Scheibel, 2007; Altman *et al,.* 2003). In addition, silk fibroin, or regenerated silk, can be processed completely in aqueous conditions; this ensures no trace amounts of harmful solvents could reach *in vivo* applications (Altman *et al*., 2003). Finally, silk degrades slowly *in vivo*, and the degradation rate can be tailored by altering β-sheet content (Altman et al, 2003, Horan *et al*., 2005).

Silkworm cocoons that comprise the raw material are made of two major products: silk and serecin. The serecin is a glue-like protein that serves to keep the cocoon together, but has been shown to elicit an

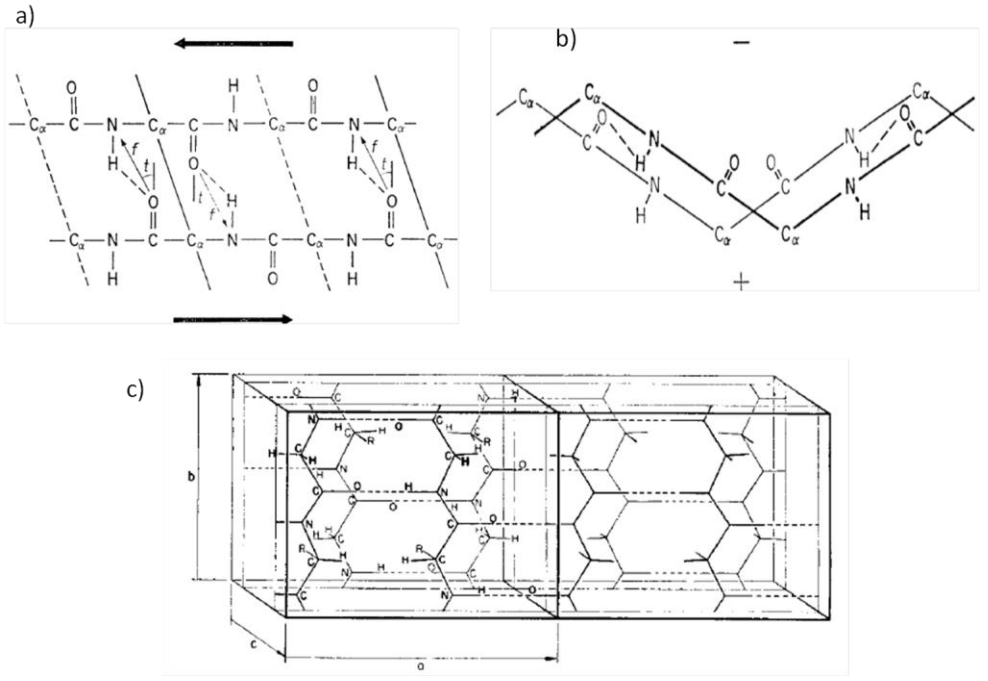

Figure 6: a) Top view of β-sheet response to shear stress (Furkawa and Takashita, 1971). b) Side view of of β-sheet response to shear stress (Furkawa and Takashita, 1971). C) 2 crystal units of silk fibroin (Marsh *et al*., 1955).

unfavorable immune response *in vivo* (Altman *et al.*, 2003). For this reason, serecin is typically removed from the silk for biomedical applications. Silk, the desired protein product for biomedical applications, has two fibroin chains, termed the light chain (25 kDa) and the heavy chain (325 kDa). The heavy chain contains mostly short chain amino acids: 45% glycine (G), 30% alanine (A), and 12% serine (S) that form a highly repetitive sequence of GAGAG $[SG(AG)_2]_8SGAAGY$ (Y=Tyrosine) (Kaplan *et al.*, 1994; Lotz and Cesari, 1979). In the chain resulting from this sequence, the alanine residues are located on one side of the silk chain, while the glycine residues line up on the opposite side of the chain; this orientation allows for hydrogen bonding between sheets. More specifically, it has been found that the sheets pack together in an anti-parallel fashion, forming a crystalline structure called the β-sheet structure or Silk II.

Another, less stable, silk structure has been found and is called Silk I. This silk structure has been observed in silk removed from the *B. mori* gland. Silk I rapidly converts to Silk II under a variety of conditions including increased temperature, applied mechanical force, and exposure to alcohols (Lotz and Cesari, 1979). While the finer details of the structure of Silk I are poorly understood because of its metastable nature, it is generally characterized as a non-crystalline, less ordered conformation.

Investigation into the structure of silk fibroin found the β-sheet structure in silk consists of anti-parallel sheets (Marsh *et al*., 1955). That same investigation determined that a crystal unit in silk fibroin consists of two anti-parallel sheets of four amino acids, resulting in an orthogonal crystal structure (**Figure 6**); however, the structure was assigned to the monoclinic space group P_{21} based on symmetry. Taking the structural basis for piezoelectricity and the unit cell into consideration, it could be possible to recreate the piezoelectric effect in regenerated silk fibroin films by increasing the β-sheet content and ordering the unit cells so they are aligned to magnify the observed effect.

Fukada and Takashita elucidated the piezoelectric polarization in the β-sheet structure under shear stress as seen in **Figure 6.** In particular, the strands interact via hydrogen bonds from N—H to C—O. Under shear stress, the polymer chains cope with the applied force by rotating between alpha carbons; the peptide bond is considered rigid. This rotation increases the distance between the N—H and C—O bonds, breaking the bond and leaving charged groups. The rotation causes predominantly oxygen to orient in one direction, and hydrogen to orient in the opposite direction. This is the dipole that forms the basis of piezoelectricity.

By applying the molecular alignment strategies mentioned earlier, piezoelectricity in regenerated silk fibroin has been demonstrated (Yucel *et al.*, 2011). A mechanical drawing technique was used to induce alignment, and shear piezoelectricity was observed. It was found that by increasing the extent of drawing, or draw ratio (λ=final length/initial length), the observed piezoelectric effect increased. This was attributed to the increased β-sheet content within the films as well as the alignment of those β-

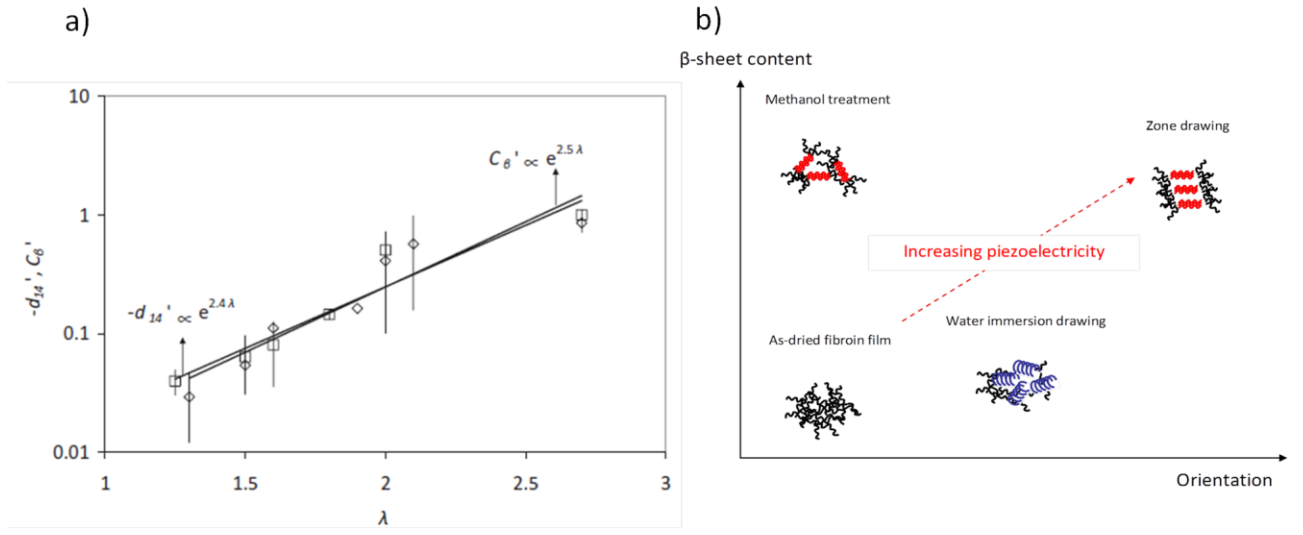

Figure 7: a) Correlation between β-sheet content and piezoelectric strain constant in silk films. B) Relationship between piezoelectric effect, β-sheet content, and β-sheet alignment (Yucel *et al.*, 2011).

sheets (**Figure 7**).

With a method to create piezoelectric silk films, the possibilities for a biocompatible, biodegradable, electrically active biomaterial can be discussed. It may be possible that a piezoelectric film could serve as the basis for a sensor or power harvester, although the properties of the film would have to be further characterized. Of interest is the possibility of these films to be used in regenerative medicine.

Piezoelectric Film Applications

Piezoelectric devices have traditionally been used as a sensing platform or power harvesting material (Anton and Sodano, 2007). Because of the inherent proportionate relationship between force and charge, piezoelectric materials have been used as strain sensors (Sirohi and Chopra, 2000). That same basic relationship between force and charge has been exploited in the converse to create sensors; piezoelectric materials will oscillate mechanically when an alternating current is applied and interaction between the device and added mass causes changes in the characteristics in the oscillations, which can be measured and correlated back to the amount of mass in a very precise way. Piezoelectric devices based on this relationship have been developed for both laboratory and field applications (Marx, 2003; Lewis *et al.*, 2005). To date, the fabrication of piezoelectric strain sensors for biomedical applications have relied on microelectromechanical (MEMs) principles and traditional semiconductor fabrication techniques. The processing solvents and materials used pose significant biocompatibility concerns. A biocompatible, piezoelectric polymer may offer a promising alternative. In a separate sensing application, piezoelectric film sensors were used to monitor respiration and heartbeat by placing a film underneath a sleeping patient (Bu *et al*., 2007). Piezoelectric silk may be applicable to research areas similar to these.

As stated earlier, bone—and more specifically collagen in bone—exhibits intrinsic piezoelectricity. Further research has suggested that this piezoelectric effect plays a crucial role in bone regeneration (Bassett *et al.*, Marino *et al.*). More recently, research has found that cells possess membrane potentials, and altering the membrane potential affects cell proliferation and differentiation (Hronik-Tupaj *et al.,* 2011; Sundelacruz *et al.*, Levin, 2009; Brighton *et al.*, 2001; McCaig *et al.*, 2005; 2009). The cells only require tens of millivolts for the membrane potential to be affected; piezoelectric silk should be capable of delivering this magnitude. By generating a biocompatible, biodegradable piezoelectric material, it could be possible to aid in bone regeneration *in vivo*. In fact, Shimono *et al*. found that piezoelectric poly-L-lactic acid improved the formation of bone in a rabbit model (1996).

Research has been conducted using basic circuit elements to apply electric fields to cells. By using either inductively or capactively coupled electric fields, cells in culture have been subjected to exogenous

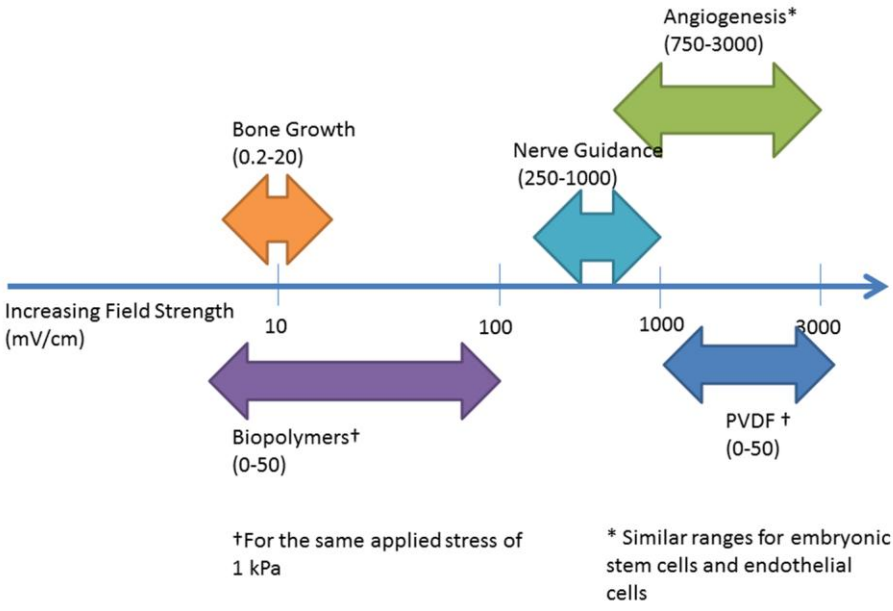

Figure 8: Electric field stimulation used for cell studies previously compared to electric fields possible with piezoelectric polymers.

electric fields (Lorich *et al.*, 1998; Chang *et al.*, 2004; Brighton and McCluskey, 1988; Hartig *et al.* 2000). These studies typically place cell culture dishes within a solenoid (inductive coupling) or between what amount to giant capacitor plates (capacitive coupling). Both methods have applied electric fields on the order of tens of millivolts per centimeter and yielded similar results; namely, cells—both bone and mesenchymal stem cells—respond to exogenous fields by increased DNA content and alkaline phosphatase expression. Other indicators included collagen I expression, calcium content, and prostaglandin levels, but varied depending on the study (Lorich *et al.*, 1998; Chang *et al.*, 2004; Brighton and McCluskey, 1988; Hartig *et al.* 2000).

There have been a couple of examples of piezoelectric collagen films used in cell studies, although these studies have been rudimentary (Silva *et al.*, 2001; Sun *et al.* 1996; Yang *et al.* 1998 and 2006). Silva *et al.* discussed the piezoelectric effect of collagen films, but did not apply any alignment techniques, resulting in properties much lower than that found in native collagen.

Collagen films created using the poling method yielded charge on plane of the film (Sun *et al.* 1996; Yang *et al.* 1998 and 2006). The authors monitored the spontaneous decay—i.e. without any applied stress—of trapped charge and found that it dropped to practically zero in days (Yang *et al*. 2006). While Yang *et al.* found that both CHO and HL-60 cells respond to the piezoelectric collagen films by increasing in calcium content and proliferation, the cell study 1) was only conducted for 45 minutes and 2) did not include mechanical cycling of the piezoelectric films. In both studies, Yang *et al.* found the films only maintained charge for 30 minutes in DMEM (Dubelcco's modified eagle medium), so the reason for short term studies most likely is the direct result of the short-term stability of the film. The latter point could be justified by the fact that the group showed that charge is maintained for at least 45 minutes, although this also highlights the fact that the piezoelectric collagen is neither truly piezoelectric nor

stable. The short-term nature of the study does not translate to the *in vivo* bone healing timescale. Lastly, the choice of a mutated cell lines means the results cannot be translated directly to primary cell lines.

Silk, in contrast to collagen, could offer improved performance with maintained biocompatibility. Through the understanding of the origins of piezoelectricity in regenerated silk fibroin, and the inherent advantages of silk as a biomaterial, it is crucial to examine the feasibility of piezoelectric silk films as a functional biomaterial. This requires two main examinations: 1) The behavior of piezoelectric silk films in biological conditions and 2) the stability of the piezoelectric effect. The following pages detail the work done to elucidate these behaviors.

Methods

Silk fibroin solution

Aqueous silk fibroin solution was prepared as described previously (Rockwood *et al.*, 2011**;** Vepari *et al.,* 2007, **Figure 9**). *Bombyx mori* cocoons were boiled in 0.02M sodium carbonate solution for 20 minutes, washed with deionized (DI) water, and allowed to dry for at least 12 hours. The silk fibroin was then dissolved in 9.3M lithium bromide solution for 4 hours to dissolve the silk. Dissolved silk was dialyzed (Molecular weight cut off 3,500) against DI water for 48 hours and centrifuged to remove any particulate. This resulted in a solution of 5-8% (w/v) silk solution.

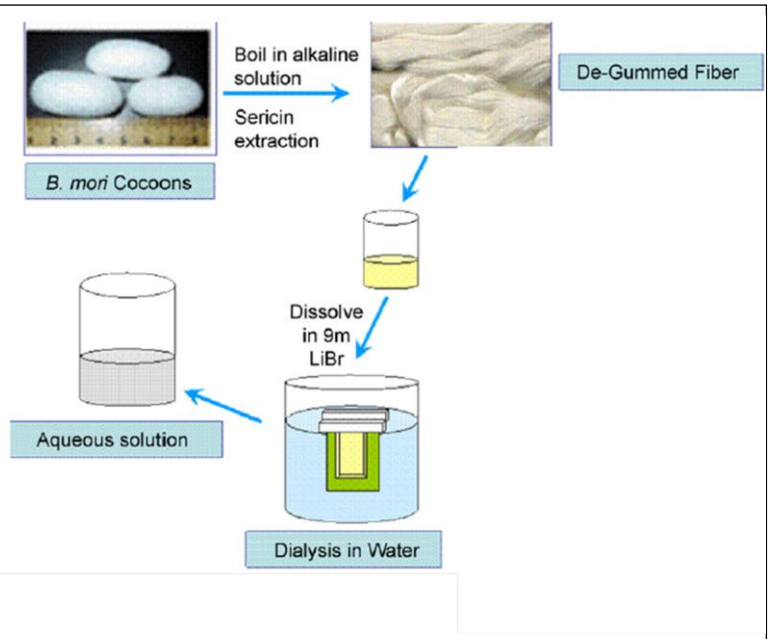

Figure 9: Processing of silk fibroin. Silk cocoons are boiled in 0.02M sodium carbonate solution for 20 minutes yielding degummed silk fibroin. Silk fibroin is dissolved in 9.3 M LiBr solution for 4 hours and dializyed for 48 hours against DI water (Vepari *et al.*, 2007).

Recombinant Spider Silk Films

Recombinant spider silk proteins were created by the University of Bayreuth as described by Huemmerich *et al.* (2004). Cloning is performed as described. The amino acid module C is first incorporated individually into the cloning vector *pAZL*. Ligation of two vectors, each containing one module, results in a lengthened protein sequence. Module sequence and protein length are controlled through this ligation process. The completed module sequence is then transferred into expression vector pET21a, and expressed in *E. coli* strain BLR(DE3).

After induction, harvested cells are lysed by sonication and cell fragments are separated by centrifugation. Bacterial proteins are precipitated upon heating and the remaining soluble silk proteins are precipitated with ammonium sulfate and harvested by centrifugation. Resulting proteins are dissolved in 6M guanidinium chloride and dialyzed against NH_4HCO_3. Soluble proteins are collected using centrifugation and are lyophilized.

Silk films

Silk films were cast using 5% silk fibroin solution in 10 cm polystyrene dishes and left to dry partially covered in a laminar flow hood. Resulting films were transparent, predominantly random coil films with a typical thickness of approximately 80 microns (μm). In the case of spider silk films, a 5% (w/v) solution was made and cast at 4°C to prevent protein aggregation and slow the solvent evaporation rate to eliminate bubbles forming in the film.

Zone-drawing

Molecular alignment was induced using a zone drawing technique as described previously (Yucel *et al.*, 2011, **Figure 10**). A film under tension is flanked by two heating elements capable of heating small regions of the film to its glass transition temperature via temperature indicator controls, while a stepper motor moves the heaters along the length of the film. The added molecular mobility induced by heating allows the film to stretch without breaking. Stretching the films pulls the α-helical silk I structure into a β-sheet silk II structure and increases alignment along the axis of the draw; an increase in β-sheet content increases the magnitude of the piezoelectricity (Yucel et al., 2011). The extent of stretching that occurs can be characterized by the draw ratio

$$\lambda = \frac{L_f}{L_i} \tag{8}$$

or the ratio of the final length to the initial length. By controlling the force applied to the film, the draw ratio can be controlled. Previous results have shown that piezoelectricity of polymers is influenced by the magnitude of the draw ratio (Yucel *et al.*, 2011, Shimono 1996).

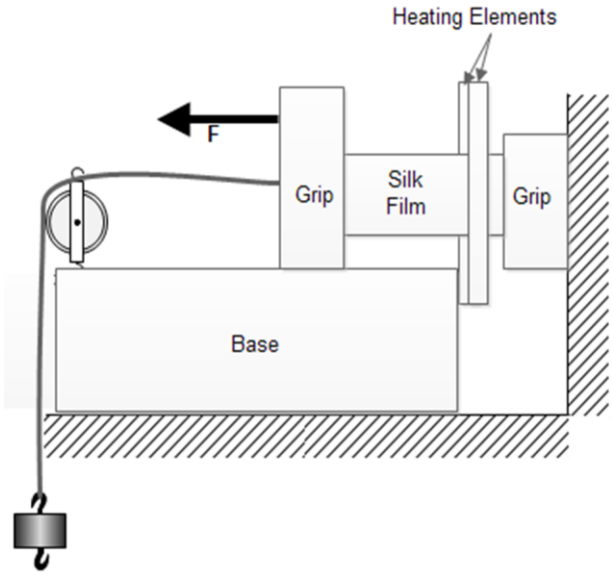

Figure 10: Zone drawing setup as described by Yucel *et al.* Silk films are stretched as they are locally heated by heating elements on either side of the film. (2011).

Post treatment of films

Methanol Bath

Water insolubility was induced using methanol baths of either 50 or 100% (v/v). Films were immersed in the methanol bath for 5 minutes, after which they were fixed to a flat surface to dry.

Water anneal

Temperature controlled water annealing was used to induce water insolubility as described previously (Hu *et al*, 2011). Here, a temperature controlled vacuum chamber was used to create high relative humidity environments. Different temperatures were chosen to examine the effect of extent of crystallization on resulting piezoelectric effect (**Figure 11**). Annealing at each temperature was allowed to go to completion as described by Hu *et al*. (2011).

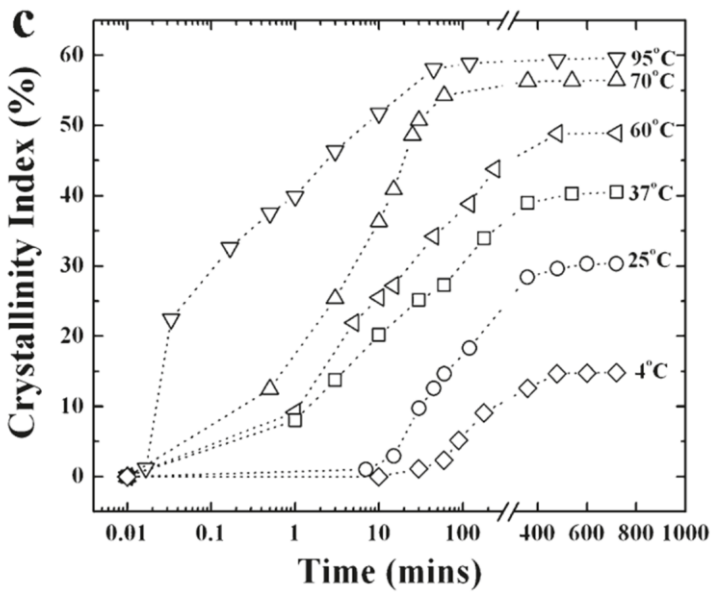

Figure 11: Effect of water anneal temperature on maximum crystallinity of silk films (Hu *et al.*, 2011).

Statistical Analysis

Minitab 15 statistical software was used to determine the significance of the difference between piezoelectric properties after post-treatments. One way unstacked ANOVA was used to compare first all treatments, and in some cases ANOVA comparisons were examined between only two treatments.

Fourier-Transform Infrared Spectroscopy (FTIR)

FTIR was used to track the relative content of secondary structures in the piezoelectric films (Yucel *et al*, 2011). In particular, the amide I and amide II bands were used to follow changes in the presence of random coil, α-helix, and β-sheet content using wavenumber assignments described previously (Yucel *et*

al, 2011, Hu *et al.*, 2006). Fourier self-deconvolution was used to determine β-sheet content in silk films as described in detail by Hu *et al.* (2006).

Thermogravimetric Analysis (TGA)

In some cases, TGA was used to determine the glass transistion temperature necessary for zone-drawing. Samples of 5 mg were used, and the temperature was ramped from 25°C to 800°C at 5°C/min. The glass transition was determined as the point where the weight change rate changed.

Wide angle X-ray diffraction (WAXS)

WAXS was used to investigate alignment of structures in piezoelectric films. The source wavelength was 0.1371 mm, pixel size was 0.158 mm, and aluminum oxide was used as a standard. Films were sampled in air at room temperature, and comparison of bands before and after zone drawing was used in conjunction with band assignments to determine alignment (Yucel *et al*, 2011; Shen *et al*., 1998, Riekel *et al.*, 1999).

Gold Sputtering

In order to measure the current and voltage produced by the piezoelectric silk, the films were coated in 100 nanometers (nm) of gold to serve as electrodes. This was performed using a Nanomaster, Inc. NSC 3000 sputter tool. The chamber reached a base pressure of 0.08 milliTorr (mT) and sputtering pressure of approximately 5 mT. Applied power was 141 Watts. As a thickness monitor, a glass slide was partially covered and placed in the chamber as well. After sputtering, the covering was removed, and profilometry was used to confirm film thickness with a Veeco Dektak profilometer.

Parylene Coating

For liquid measurements (described later), thin films of parylene were used to achieve conformal coatings of insulating layers on materials. A Specialty Coatings Systems PDS2010 parylene coater was used. In this system, 6.5 g of parylene precursor was used to achieve film coatings of approximately 3 μm.

Dynamic Mechanical Analysis (DMA)

Current

The fundamental equations to characterize piezoelectric materials can be seen in **Equations 2 and 3**. Before discussing how the experimental setup functions, these equations will be rewritten in terms of measurable variables. First consider **Equation 2:**

$$P_i = d_{ij} X_j \tag{2}$$

It has been established that zone drawing induces shear piezoelectricity, so more specifically,

$$P_1 = d_{14} X_4 \tag{9}$$

Here the subscript 1 refers to the direction of the generated polarization, which here is perpendicular to the plane of the film, while 4 refers to the shear force applied. Polarization (P) is defined as charge per area, and stress (X) is force per cross-sectional area. These can be substituted into the above equation to yield:

$$\frac{Q}{A_E} = d_{14} \frac{F}{A_{XS}} \tag{10}$$

Here, Q is charge, A_E is the electrode area (gold-coated area), F is force, and A_{XS} is the cross-sectional area. Current is the time derivative of charge, so

$$\frac{d}{dt}\left(\frac{Q}{A_E}\right) = \frac{d}{dt}\left(\frac{Fd_{14}}{A_{XS}}\right) \quad (11)$$

In order to determine the derivative, the applied force must be considered. In the DMA setup, a sinusoidal force is applied, and a sinusoidal current results:

$$F(t) = F_0 \sin(\omega t) \quad (12)$$
$$Q(t) = Q_0 \sin(\omega t + \phi) \quad (13)$$

Where the 0 subscript denotes maximum values, ω represents frequency, and ϕ represents phase lag. Taking the time derivatives of these yields:

$$\frac{dF(t)}{dt} = (F_0 \omega \cos(\omega t)) \quad (14)$$
$$\frac{dQ(t)}{dt} = \left(\frac{dQ_0}{dt}\right)(\omega \cos(\omega t + \phi) \quad \text{and} \quad \frac{dQ_0}{dt} = I_0(t) \quad (15)$$

Equations 15 and **16** can then be inserted into **Equation 12**.

$$I_0(\omega cost(\omega t + \phi)) = d_{14}(F_0 \omega \cos(\omega t)) \quad (16)$$

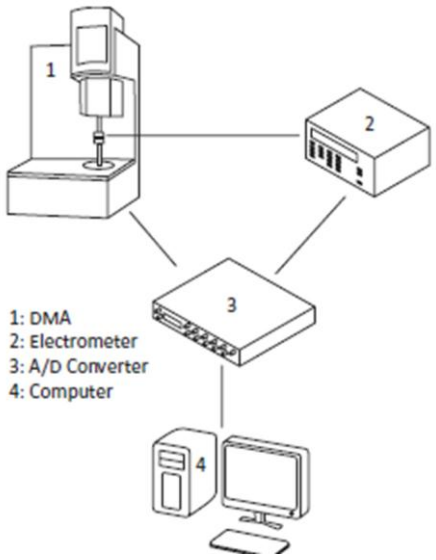

Figure 12: Modified DMA setup. The DMA and electrometer interface with an A/D converter and the data are recorded using a computer. (Yucel *et al.*, 2011).

Now, in order to calculate the d_{14} constant, the maximum value for both the current and force are considered, which will occur when the cosine functions equal 1. Although this will occur at different positions, the maximum force will cause the maximum current, and this is why the maximum values are considered together. The final equation, rearranged to solve for the piezoelectric strain constant:

$$d_{14} = \left(\frac{I_0}{A_E}\right) / \left(\frac{F_0}{A_{XS}}\right) \quad (17)$$

Each of the above variables can be measured.

The current and force are measured using a modified dynamic mechanical analyzer (DMA). Typically, DMA measures stress and strain, but in this modified setup an electrometer (Kiethley) is added in series so that the DMA measures strain and current. The following paragraphs describe how this setup is used.

First, a PVDF standard is used to calibrate the instrument. In the first step, the DMA is used to apply sinusoidal force, and the current is measured directly from the electrometer using a data acquisition unit (Measurement Computing, 1208-LS). The electrometer is capable of measuring current values as low as femtoamperes in some cases. An electrometer is "essentially a voltmeter with a high input impedance that can be used to measure low current levels" (Tucker). By maintaining a high current source impedance of 1 teraohm and higher, the noise gain remains low and the signal-to-noise ratio can remain large even for small measured currents. Using data from the electrometer, the average peak current is calculated.

Next, the current is recorded as stress through the DMA's TA Orchestrator software. The value is measured over 3 orders of magnitude and shows a linear relationship between electrometer value and stress readout. The force applied is simultaneously recorded, and the current, force, and sample dimensions are used to calculate the d_{14} constant for PVDF, which is compared to literature to ensure the system functions properly.

After ensuring the system functions properly, conversion factors between the force component of the stress and current are calculated for each order of magnitude. A typical conversion value for electrometer readings on the order of 10^{-10} is $1.3x10^{-10}$.

In order to measure the current from silk samples, drawn films were cut 45 degrees from the direction of alignment and coated with 100nm of gold on both sides. Sample thickness, width, and length were recorded. With the calibration complete, silk samples were then placed in the instrument so that the alignment was 45 degrees from perpendicular; in this way a shear force is applied. The "stress" (which is actually current) and force are recorded and converted to current using the conversion factor. For each film, applied strains of 0.01, 0.025, 0.05, 0.075, and 0.1 percent strains were used. Then, plotting the stress against the average peak current normalized to the electrode area yields a slope which is the d_{14} value.

Voltage

As with **Equation 2**, **Equation 3** can also be rewritten in terms of measureable variables.

$$E_1 = g_{14} X_4 \tag{3}$$

E is the electric field, which is defined as voltage over distance, and the stress X is again force per cross-sectional area. Substituting:

$$\frac{V}{T} = g_{14} \frac{F}{A_{XS}} \tag{18}$$

T denotes film thickness. The voltage and force are sinusoidal and can be written as:

$$F(t) = F_0 \sin(\omega t) \tag{19}$$
$$V(t) = V_0 \sin(\omega t + \phi) \tag{20}$$

The maximum values are considered, which occurs when the sine terms equal 1. Substituting the maximum values into **Equation 3** and rearranging for g14 yields

$$g_{14} = \left(\frac{V_0}{T}\right) / \left(\frac{F_0}{A_{XS}}\right) \tag{21}$$

Again, each of these values can be measured.

The voltage measurements were also carried out using the DMA. Here, however, rather than use an electrometer, a commercial-off-the-shelf (COTS) ultra-low input bias instrumentation amplifier (Burr-Brown INA116A) was connected to a data acquisition unit (DAQ) to record the voltage. A known gain can be used for the amplifier, and the recorded voltage can be corrected to reflect the raw voltage generated by the film. Again, the average peak voltage and average peak force were used to calculate the piezoelectric voltage constant.

Liquid measurements

The electric field generated in the presence of solvent was investigated using a DMA immersion fixture, and the experimental setup can be seen in **Figure 13.** In order to simulate *in vivo* like conditions, 1x phosphate-buffered saline (PBS) was used as the solvent. The premise of the design can be thought of as creating a large capacitor where the solvent between the silk film and reference electrode is the dielectric material.

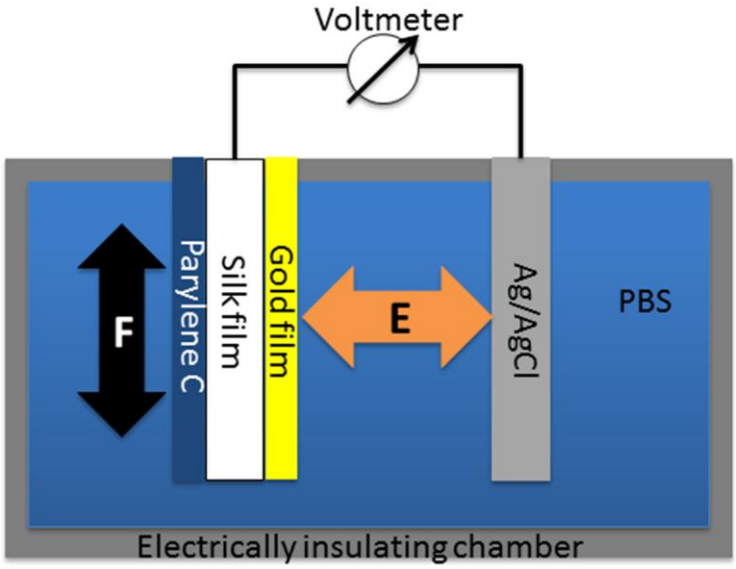

Figure 13: Experimental setup for liquid measurements. A silk film coated in gold and paralyne is clamped in the DMA and immersed in a bath of 1x PBS. An instrumentation amplifier and voltmeter are then used to measure the potential difference between the sample and a non-polarizable electrode.

First, silk films water-annealed at 60°C were coated with a layer of gold (conductor) on one side, while the opposite side is coated with parylene (insulator). Note that covering one side of the film with an insulator does not alter the piezoelectric effect, but merely prevents interaction of that side with the solvent environment.

Next, consider the DMA chamber design. All metal portions of the DMA clamps were coated with parylene to prevent any short-circuits, while the rest of the fixture consisted of electrically insulating plastic. A non-polarizable silver-silver chloride (Ag/AgCl) electrode (Harvard Apparatus) was placed in the immersion fixture 1.75 cm from the silk film surface. Connecting an instrumentation amplifier and voltmeter to the gold side of the silk film and the Ag/AgCl electrode in conjunction with the known distance between plates allows for the calculation of the electric field generated (the solvent closes the circuit).

As a control, as-cast silk films—meaning no piezoelectricity—were coated as described. A sinusoidal force was applied to film at a frequency of 0.5 Hz, while the voltage was measured. The clamps that mechanically move will inevitably be in contact with and disturb the solvent. This movement will cause some movement of the ions in the solvent, which could be large enough to be measureable. Establishing a baseline of the effect of the system itself is critical, and any sinusoidal voltage measured here will be considered the noise of the system.

With a baseline for the system established, piezoelectric silk films were investigated using the same experimental parameters as those used in the control samples while the voltage was recorded.

Lifetime analysis

The stability of the piezoelectric effect in silk films was examined. Here, a modified bioreactor (Kluge *et al.*, 2006) was used to cycle films continuously using a stepper motor (**Figure 14**). The film was again connected to an instrumentation amplifier and DAQ unit. Two Visual Basic programs were created, one to control the motor and the other to record voltage. The motor control program cycled the motor between two user-defined points at 0.35 Hz, resulting in a square wave of force applied to the film. In the absence of a load cell in the setup, films were cycled with a large enough strain that it was visible, which was about 5% strain. Every 10 cycles, the total cycles completed were printed to the screen with a time stamp, and this data was saved to a text file.

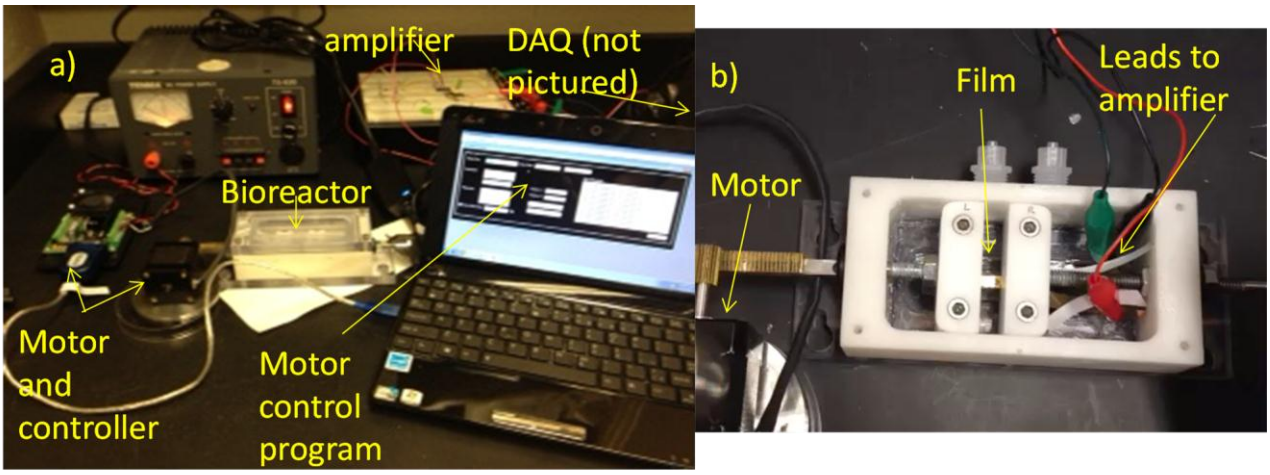

Figure 14: a) experimental setup for lifetime analysis. b) Top view of inside of bioreactor with film.

The voltage program used was modified from the Measurement Computing ULA01.vb program accompanying the hardware. This program, which originally printed the present value from a given analog input channel to the screen, was modified to run on a timer. The user defined the number of data points to collect, and the time between collections. Typical parameters were 200 data points (collected at 10 Hertz) collected every 24 minutes. For each interval, the voltage value was recorded and time stamped and saved to a text file.

Using the time stamps, the voltage and cycle number could be correlated. To present the data, the average peak- to-peak voltage within the first 100 cycles was used as the "initial" voltage. Then, all subsequent peak-to-peak voltages were normalized to the initial voltage, and plotted against the cycle number. The film was considered to no longer be piezoelectric when the relative peak to peak voltage was approximately equal to the level of noise in the measurement.

Enzymatic degradation

Films were subjected to enzymatic degradation by α-chymotrypsin in order to determine if the films degrade similarly to as-cast films. A 4 mg/mL solution of α-chymotrypsin (Sigma-Aldrich) solution in PBS and 80mM HCl was added to films and incubated for 3 days at room temperature, replacing the enzyme

after 1.5 days. After 3 days, the films were rinsed three times with DI water and allowed to dry. Dried films were investigated using atomic force microscopy (AFM).

Atomic Force Microscopy

AFM measurements were taken using a Veeco Dimension V and a phosphorous-doped silicon cantilever (Veeco RTESP). The cantilever was 115-135 μm long with a resonant frequency between 264 and 302 kHz and a spring constant of 20-80 N/m. All measurements were taken in tapping mode, and height maps were considered.

Results

Structural Indications of Piezoelectricity

FTIR and WAXS data were collected to confirm that zone-drawn films possessed similar structural characteristics to those reported by Yucel *et al* (2011). **Figure 15** displays FTIR spectra of the amide I band of films with increasing draw ratio. The amide I band peak shifts from 1641 cm^{-1} for as-cast films toward 1624 cm^{-1} as the draw ratio increases, matching the results found in literature (Yucel *et al.*, 2011). This indicates that as λ increases, the secondary structures present in the film shift from

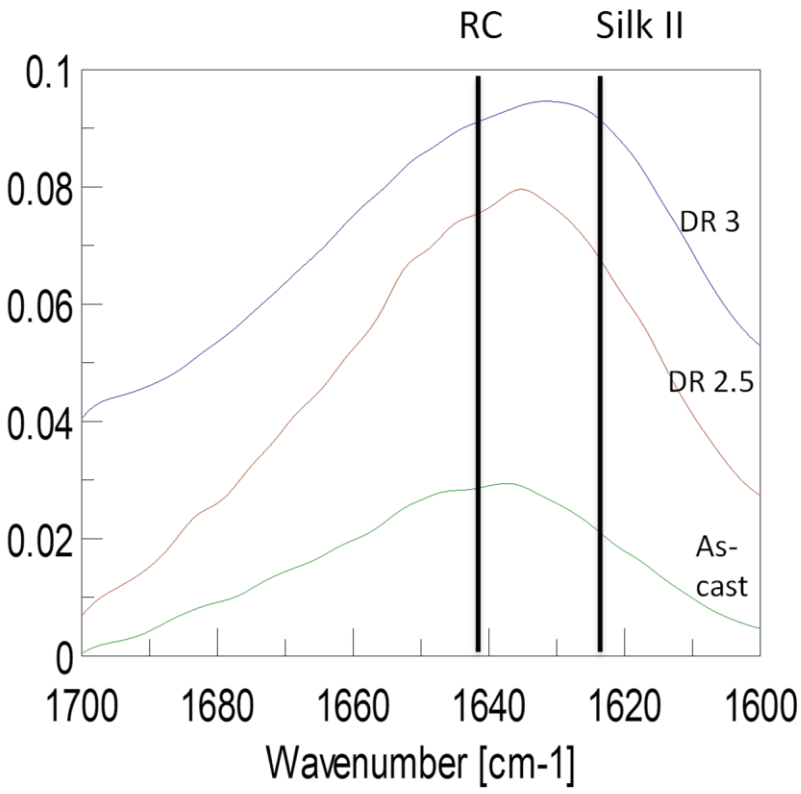

Figure 15: FTIR spectra of silk films with increasing draw ratio. The markers "RC" and "Silk II" indicate the wavenumbers associated with the random coil and silk II structure (β-sheets), respectively. Moving from the bottom spectrum to the top, the draw ratio, DR, increases. At the same time, the peak shifts from random coil towards the silk II region.

predominantly random coil to β-sheets, which is one key component to silk piezoelectricity.

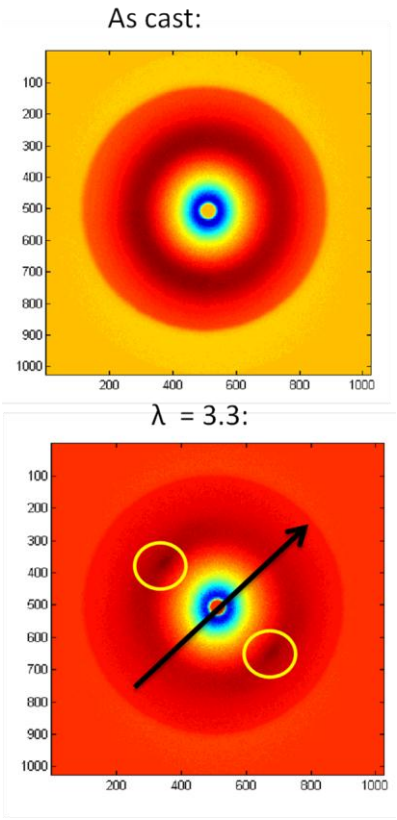

Figure 16: WAXS results : WAXS results. *Top:* As cast film. Diffuse rings indicate random alignment. *Bottom:* Film with 3.3 draw ratio, circles highlight appearance of 020/002 plane, and arrow indicates direction of alignment. Appearance of the 020/002 plane indicate alignment (Shen *et al.*, 1998). Images courtesy of Dr. Peggy Cebe.

Figure 16 contains images of WAXS data collected from *B. mori* piezoelectric films. In the top figure, as-cast films show only diffuse rings, indicating random alignment. Zone drawing led to a transition from amorphous structure—indicated by diffuse rings—to an aligned structure, indicated by the appearance of the 200/020 planes, which are circled for clarification (Yucel *et al.*, 2011; Shen *et al.*, 1998). This, in combination with the FTIR results, confirms the structural components necessary for the piezoelectric effect are present.

Enzymatic Degradation

Films subjected to enzymatic digestion with α-chymotrypsin were investigated using AFM, and the results can be seen in **Figure 17.** First, consider the control samples. Films soaked in PBS do not show any defining characteristics. In addition, as-cast films digested by enzyme show random orientation and pitting. Considering now the piezoelectric silk digested by enzyme, a few noticeable differences arise. First, block-like structures appear to be exposed, which are a few microns in either direction. The dimensions correspond to the dimensions of β-sheet structures found by Numata *et al.* (2010). Secondly, defined channels appear that match the direction of the applied force during the zone-drawing method and corresponding alignment.

The appearance of the block structures appears to indicate crystalline packing. These results further support the combination of crystalline structure and alignment in piezoelectric silk.

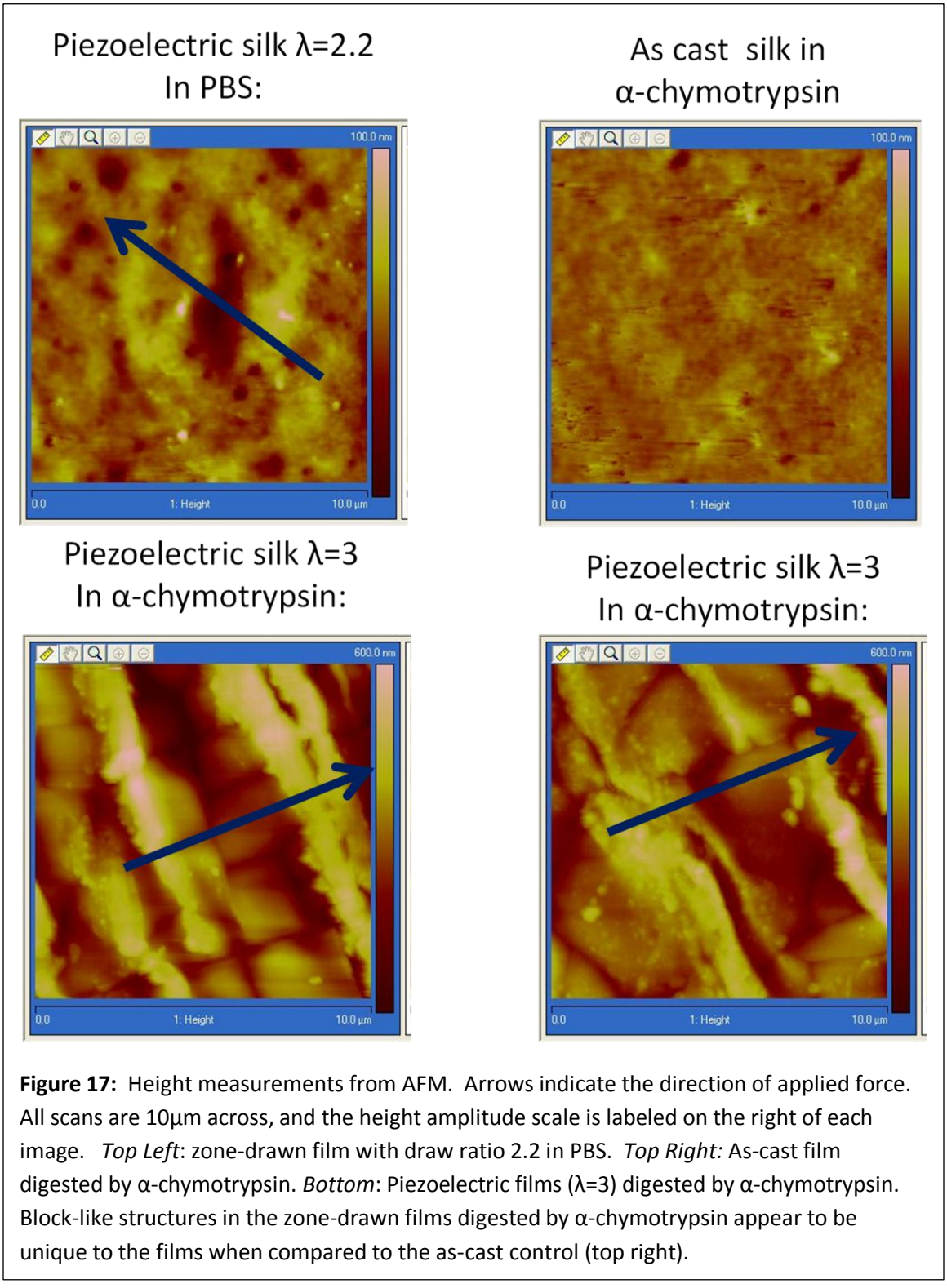

Figure 17: Height measurements from AFM. Arrows indicate the direction of applied force. All scans are 10µm across, and the height amplitude scale is labeled on the right of each image. *Top Left*: zone-drawn film with draw ratio 2.2 in PBS. *Top Right:* As-cast film digested by α-chymotrypsin. *Bottom*: Piezoelectric films (λ=3) digested by α-chymotrypsin. Block-like structures in the zone-drawn films digested by α-chymotrypsin appear to be unique to the films when compared to the as-cast control (top right).

Piezoelectric current measurements

Films were tested using the DMA as described to measure the current generated under applied stress. **Figure 18** displays the current normalized to electrode area (area coated in gold) with increasing stress; the slope is the piezoelectric strain constant, d_{14}. The trend of increase in piezoelectricity with increasing draw ratio is consistent with previous results, and is indicated by the increasing slope.

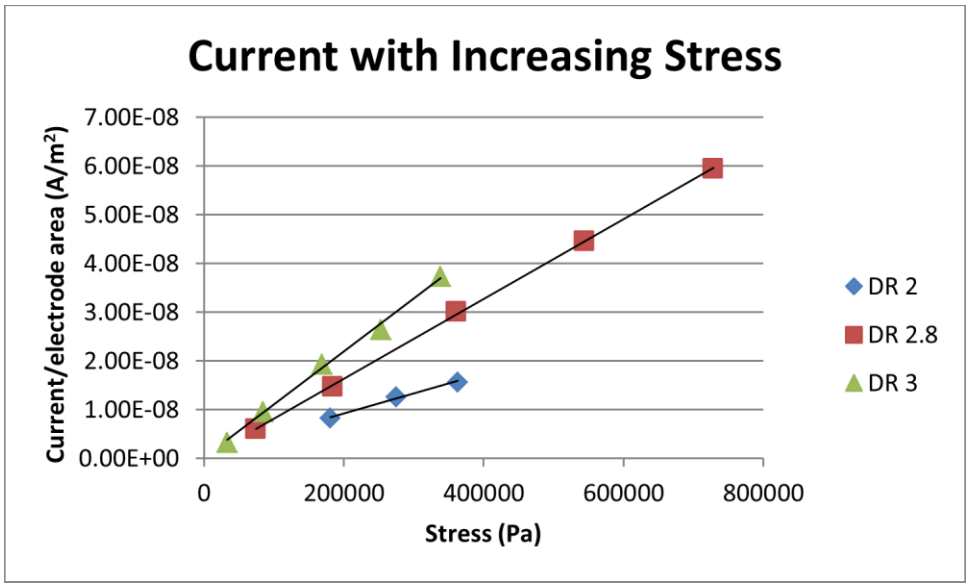

Figure 18: Current generated by piezoelectric films of different draw ratios with increasing stress. Each line tracks the piezoelectric response of a film with a given draw ratio, marked DR. By comparing the stress applied to the current generated normalized to the electrode area (area coated in gold), the slope of the curve is the piezoelectric strain constant d_{14}.

Voltage Measurements

After confirming the current generated by piezoelectric silk films compared to previous results, the voltage generated by the films was measured. As seen in **Figure 19**, a similar trend to the current constant can be observed for the voltage constant with increasing draw ratio. As was observed with the current, the voltage resulting from applied stress increased with increasing draw ratio.

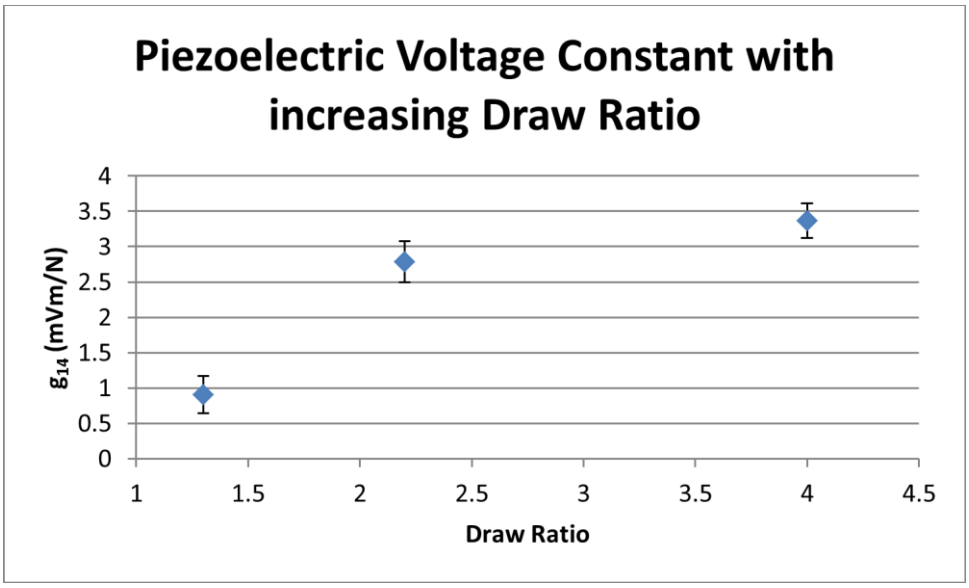

Figure 19: Piezoelectric voltage constant for silk. Increasing stress was applied to films of different draw ratios and the voltage was recorded. The stress and electric field were then plotted, and the slope of the line is the piezoelectric voltage constant, g_{14}. The value of g_{14} is plotted for different draw ratios. (n=3).

Effect of Post-Treatment on Piezoelectricity

First, consider the water-annealing treatments at different temperatures. Films were tested over a range of strains, and the slope yields d_{14}. For films of the same draw ratio differing only in the water anneal temperature, the effect can be seen in **Figure 20**. The largest effect was in the films water annealed at 60°C.

Films of different draw ratios were tested and the values of their slopes were plotted (**Figure 21**). It appears water annealed treatments improved the piezoelectric strain constant, with the difference between the water annealed films and no post-treatment significant, as determined by ANOVA ($p = 0.015$). The difference between 60 and 90°C treatments, however, was not significant ($p = 0.13$). Methanol treatments did not appear to improve the piezoelectric effect (**Figure 21**) and were not used in further experiments.

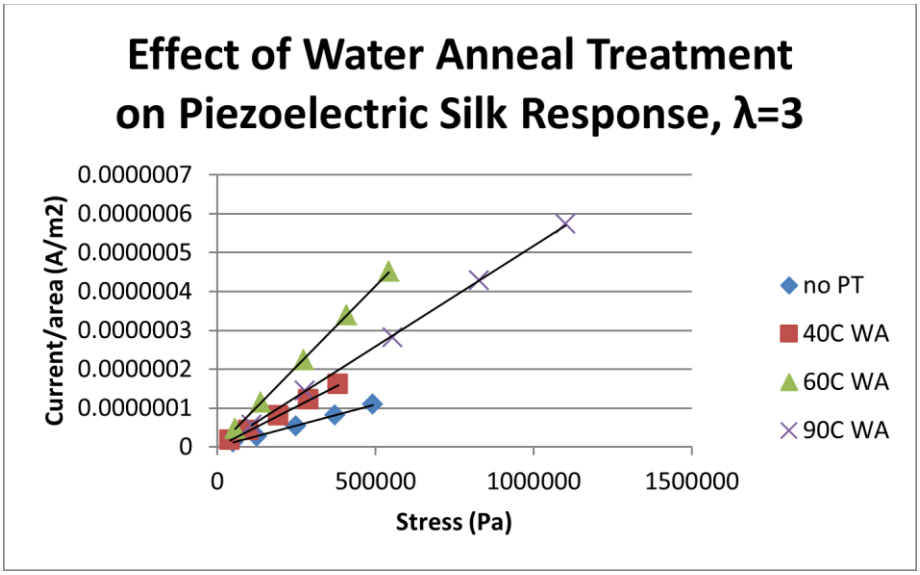

Figure 20: Current with increasing strain for films with a draw ratio of 3 water annealed at different temperatures. Films with a draw ratio of 3 were water annealed at 40, 60, and 90 °C, after which the piezoelelectric effect was established. Here, the current generated with increasing stress is plotted, and the slope is the piezoelectric strain constant, d_{14}. For comparison, a film with a draw ratio of 3 and not post-treated (no PT) is added for reference. The water annealing processes improves the observed piezoelectric effect as indicated by the increasing slope compared to no PT.

The potential difference across the thickness of the post-treated films with a draw ratio of 3 was measured to calculate the piezoelectric voltage constant, g_{14} (**Figure 22**). As expected based on the current values, the voltage generated was also preserved during the post-treatment step.

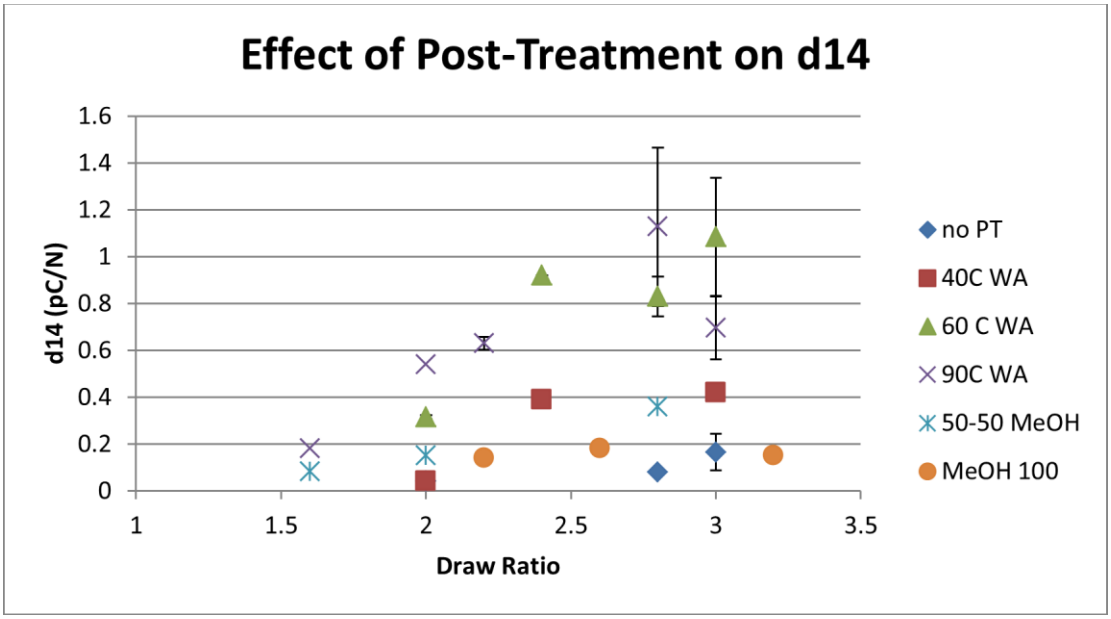

Figure 21: Effect of post treatment on the piezoelectric strain constant, d_{14}. No PT indicates no post-treatment was applied. WA indicates water anneal treatments at given temperatures and MeOH 50-50 is a 50% methanol bath treatment for 5 minutes, while MeOH 100 indicates bath immersion for 5 minutes in undiluted methanol. (n= 2 to 6).

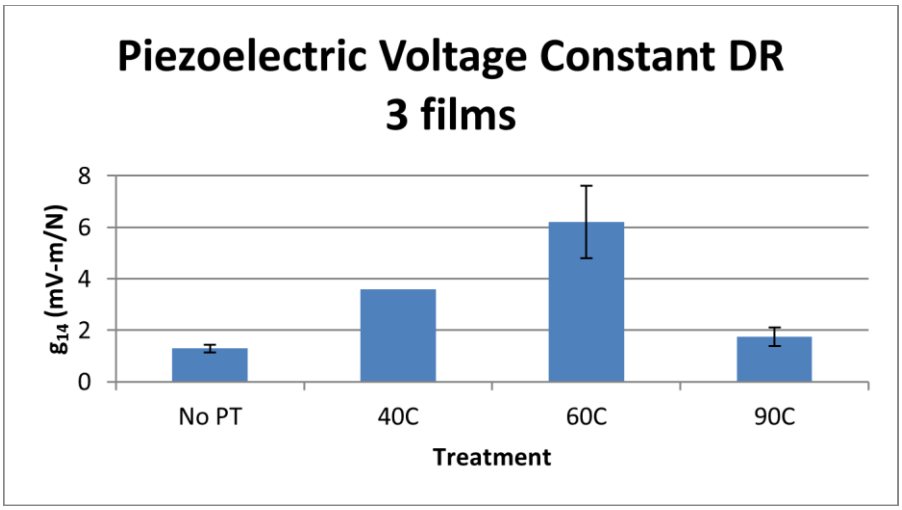

Figure 22: Effect of post treatment on the piezoelectric voltage constant, g_{14}. All films tested had a draw ratio of 3 (n=3).

Lifetime of Films

Piezoelectric silk films were investigated for their stability. The relative voltage of the films is plotted with increasing cycle number in **Figure 23**, where each film's voltage is relative to itself. From the individual films, the average relative voltage with cycle number was calculated as plotted in **figure 24**. All films maintained a measureable voltage for 120,000 cycles, after which film stability varied more between samples. As explained in the Methods section, the applied strain was about 5% for dry films, which is much larger than used in DMA measurements, and the applied stress was much larger than the parameters that would most likely be used in dry applications. Cycling the films at lower stresses may improve the lifetime of the films.

The average aging rate can be calculated from the data using the following relationship (Glynne-Jones *et al,* 2001):

$$aging\ rate = \frac{(V_2 - V_1)}{\log(t_2) - \log(t_1)} = \frac{(0.5-1)}{\log(130610) - \log(1)} * 100 = -9.8\%$$

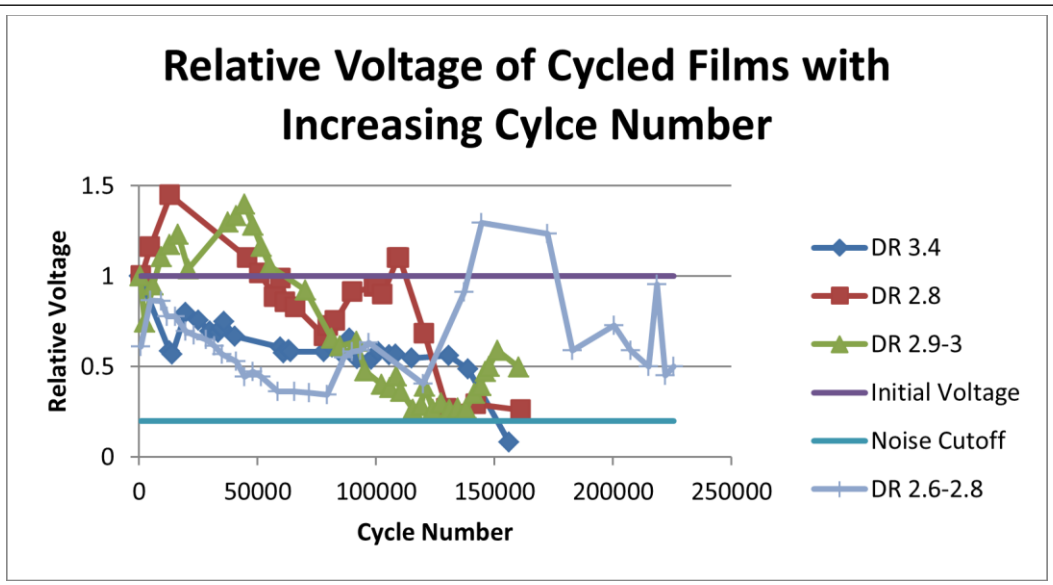

Figure 23: Relative voltages of each film investigated. The draw ratio or draw ratio range is indicated for each sample, and the initial voltage and noise cutoff are added for reference. Points indicate data values, while the lines serve as a guide between points.

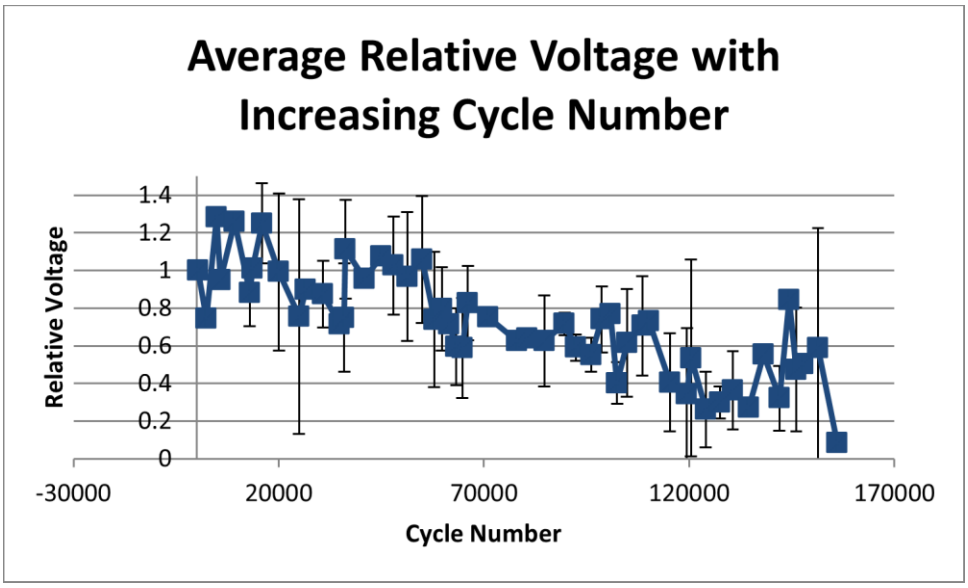

Figure 24: Average relative voltage with cycle number (n=4).

This is of course a relative approximation given the variation between samples, but it does give a baseline indication of the performance loss that can be expected, as well as an idea of the timeframe in which the film will maintain its piezoelectricity.

Liquid Measurements

A viable functional biomaterial needs to perform in aqueous environments. For this reason, films were tested in a bath of PBS. First, control films of as-cast silk were tested in the liquid to establish a noise baseline that includes both electrical noise and mechanical noise from the moving clamps. **Figure 25** shows the amplified noise in the system. The films were cycled at 0.5 Hz, meaning one complete cycle takes 2 seconds. From the noise, a sinusoidal response was not observed.

Next, a piezoelectric silk film was tested. The film was tested at 3 different strain rates—3, 5, and 7 percent—again to confirm the linear relationship between applied force and resulting electrical properties. First, consider the 5% strain values in direct comparison with the noise (**Figure 26**). Now, a sinusoidal voltage is easily distinguishable, having 0.5 Hz frequency. **Figure 27** shows the voltage response of the film at the different strains, all run at the same frequency; the phase is arbitrary.

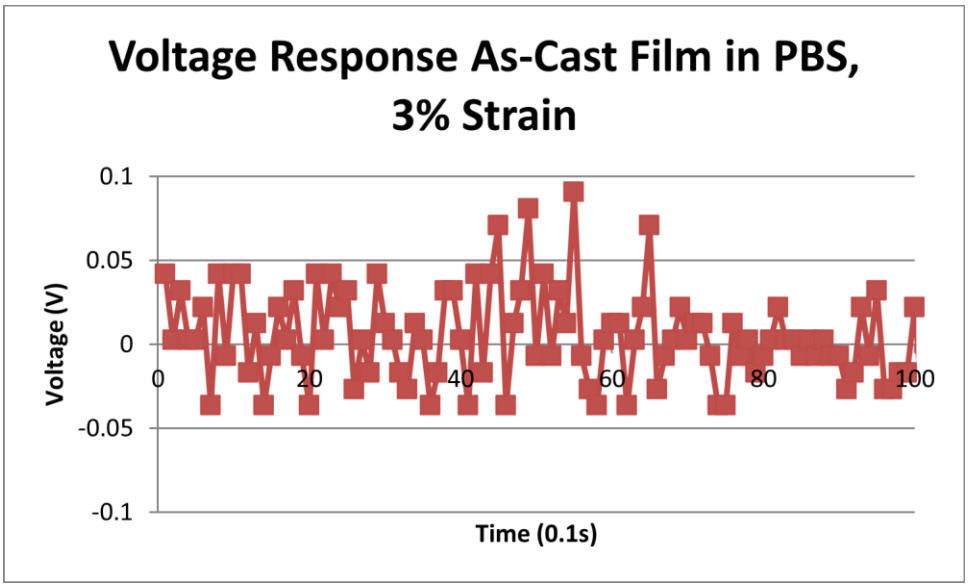

Figure 25: Noise of the system at 0.5 Hz in PBS while interrogating an as-cast silk film.

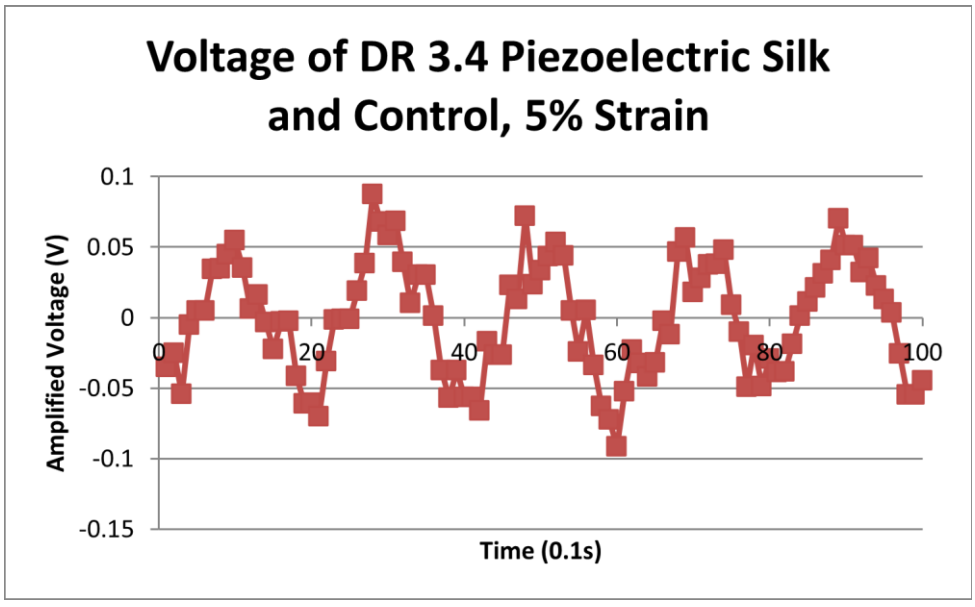

Figure 26: Voltage generated by silk film with draw ratio 3.4 in PBS under 5% strain.

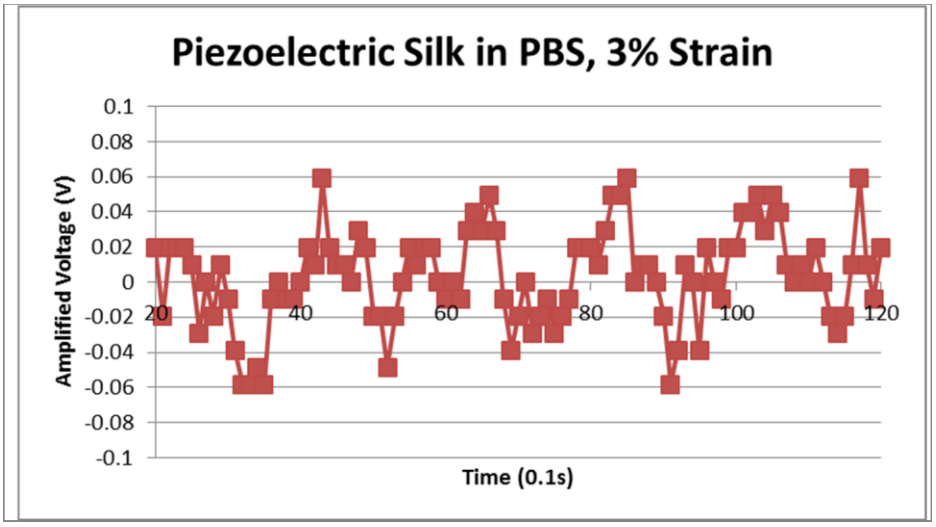

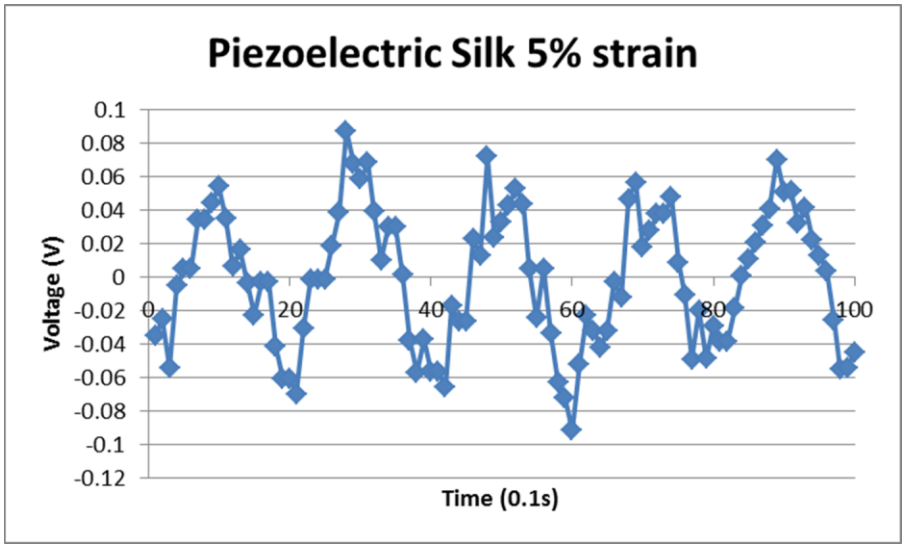

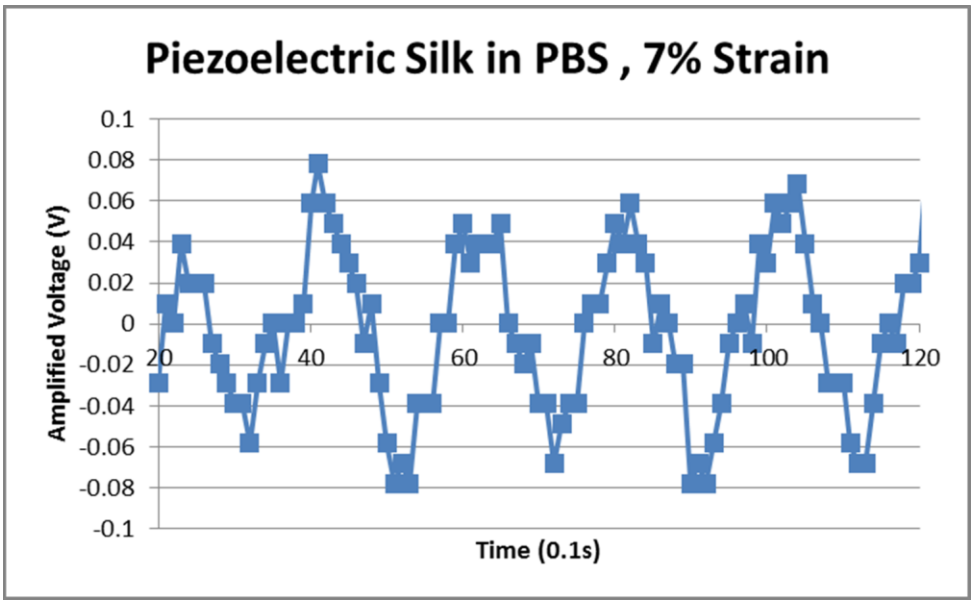

Figure 27: Response of piezoelectric silk (λ=3.4) with increasing stress.

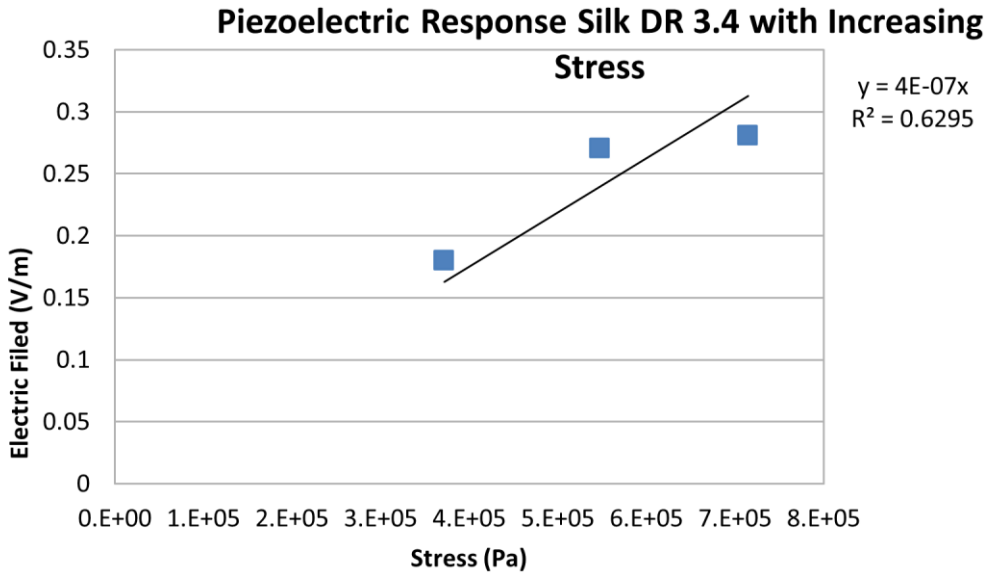

Figure 28: Piezoelectric silk response in PBS based on applied stress and average peak voltage.

The average peak voltage for each strain was calculated, and with a known applied stress and distance between the sample and reference electrode, **Figure 28** was generated. As expected based on **Figure 27**, there was an increase in response with increased applied stress. It is assumed that at zero applied force, the electric field is zero, as suggested in **Equation 3**. The response was linear between 3 and 5 percent, and in fact if only these points and the origin are considered, the correlation becomes much stronger ($r^2 = 0.985$). However, at 7%, the response no longer agrees to the values of the lower strains. At this point, the material properties of the film have changed, so that the mechanical stress-strain

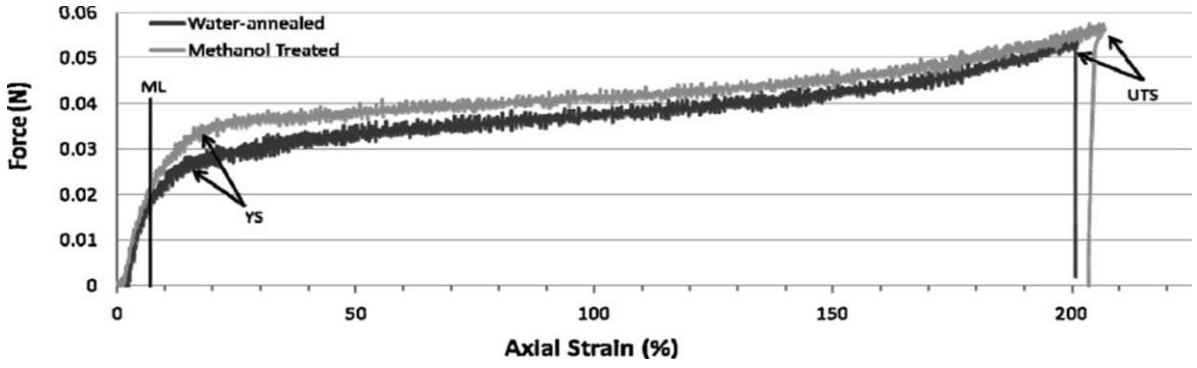

Figure 29: Mechanical properties of hydrated silk (Lawrence *et al.*, 2010). Note that 7% strain is approximately at the "ML" line ("modulus line"), which for water-annealed silk is at the end of the linear region.

properties are no longer linear. Applications using piezoelectric silk films will then need to be less than 7% in order to accurately predict the film performance.

The slope of the curve in **Figure 28** is similar to the g_{14} constant (piezoelectric voltage constant). While a direct comparison between the values is not appropriate, it is clear that in liquid, a very small electric field is present. The electric field produced for these films is 1.7, 2, and 2.7 mV/cm for 3, 5, and 7% strain, respectively.

Discussion

Piezoelectric Silk for Biomedical Application

Silk films display piezoelectric properties, and water-insolubility treatments improve the effect. Both the piezoelectric strain constant, d_{14}, and the piezoelectric stress constant, g_{14}, improved after water-annealing, with the most improved performance coming from films treated at 60°C. The magnitude of the piezoelectric effect can be modulated by tuning the processing parameters, which may be useful for applications. As seen in **Figure 29**, as the water-annealing temperature increases, so does the film

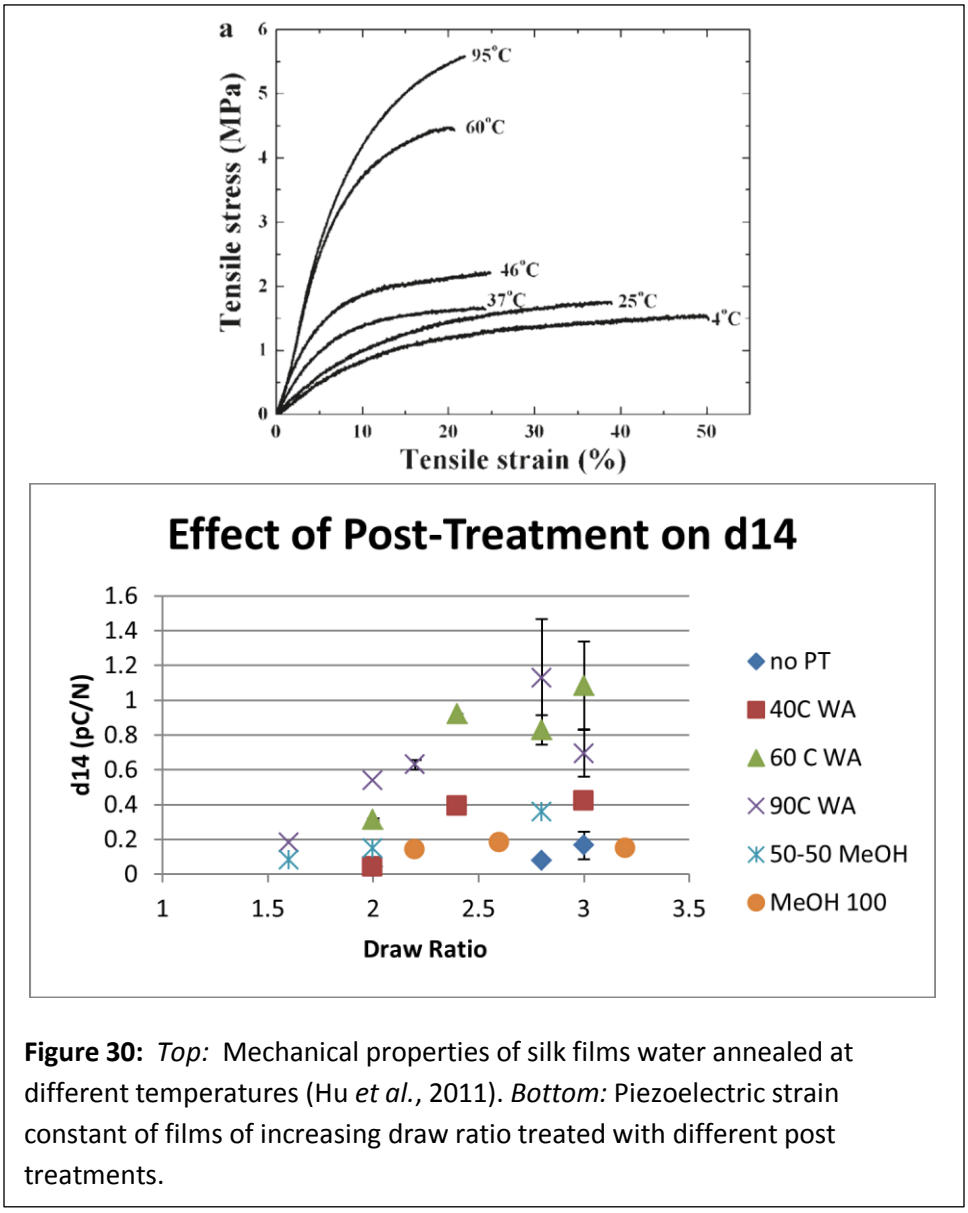

Figure 30: *Top:* Mechanical properties of silk films water annealed at different temperatures (Hu *et al.*, 2011). *Bottom:* Piezoelectric strain constant of films of increasing draw ratio treated with different post treatments.

stiffness. This information, in conjunction with the piezoelectric constants at different draw ratios, can be used to choose parameters that will yield the most desirable film properties. For example, it is known that cells respond to substrate stiffness, so piezoelectric silk films used for cell studies will need to have a stiffness appropriate for the given cell type (Yeung *et al.*, 2005; Discher *et al.*, 2005).

Piezoelectric silk films maintain piezoelectricity for at least 130,000 cycles, after which stability varies from sample to sample. **Figure 30** shows the aging rate of silk films in comparison to collagen and PZT (lead zirconate titanate) (Yang *et al*., 2006; Glynne-Jones *et al.*, 2001). First, the collagen films examined in the study by Yang *et al.* are bioelectrets, meaning the films have been poled. The resulting permanent polarization drops quickly in the first 5 days; it should be noted that the films are not cycled

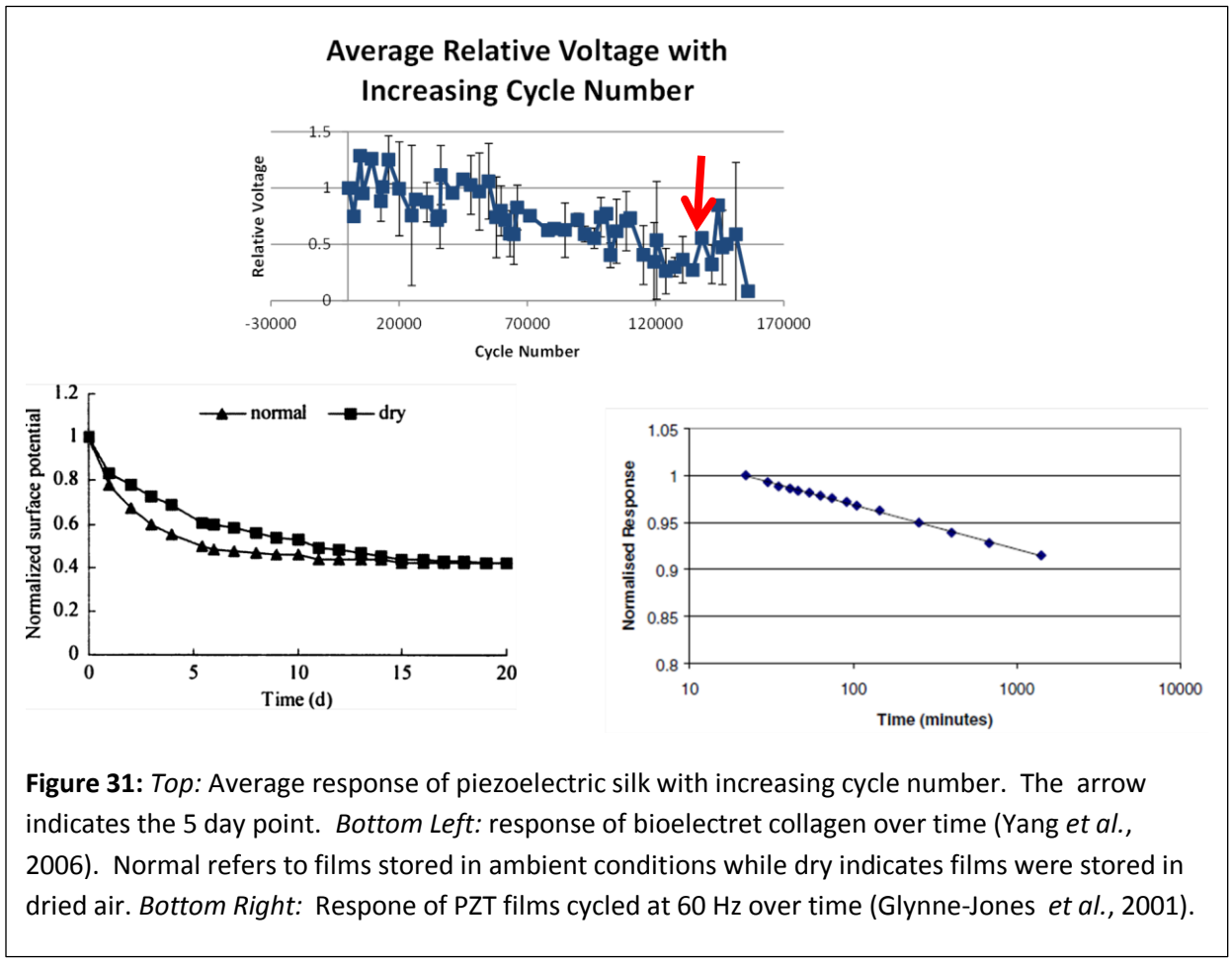

Figure 31: *Top:* Average response of piezoelectric silk with increasing cycle number. The arrow indicates the 5 day point. *Bottom Left:* response of bioelectret collagen over time (Yang *et al.*, 2006). Normal refers to films stored in ambient conditions while dry indicates films were stored in dried air. *Bottom Right:* Respone of PZT films cycled at 60 Hz over time (Glynne-Jones *et al.*, 2001).

during this time; the films display permanent polarization. (2006). At the other extreme, PZT was cycled at 60 Hz and lost less than 10% of its performance in over 3 million cycles (Glynne-Jones, 2001). PZT, however, is typically used in devices rather than applications requiring biocompatibility.

Comparing piezoelectric silk to piezoelectric collagen, the basis of the effect differs. Silk possesses shear-induced polarization, meaning it only polarizes under applied stress. Collagen, as a bioelectret, possesses a partially stable trapped polarization as a result of the applied electric field used to align the dipole in the film. As a result, the collagen surface potential is short-lived and only lasts for minutes in the presence of liquid (**Figure 31**). Such a short-term charge has very limited use in biomedical engineering. In fact, cell studies culturing cells on bioelectret collagen were only carried out for 45 minutes because of the short-lived polarization of the film. A 45-minute effect for biomedical

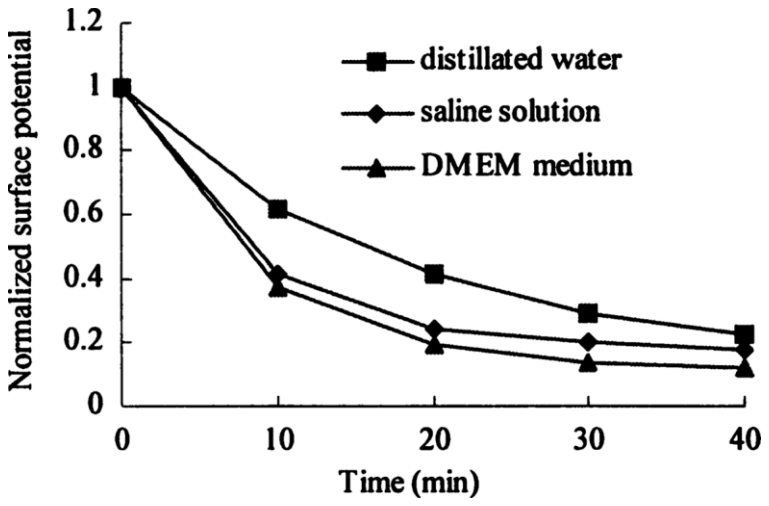

Figure 32: Charge decay of electrically poled collagen films (Yang *et al.*, 2006). The magnitude of the surface potential decreases significantly in the presence of ionic liquid, and the time scale has shifted from days to minutes when compared to the response of a dry film in **Figure 30**.

applications is impractical, and calls into question the designation of "electret" as defined by Mascarenhas that "a substance is said to be an electret if the decay time of its stored polarization is long in relation to the characteristic time of experiments performed on the material" (1987, p 324). Silk, on

the other hand, exhibits shear-induced piezoelectricity, so polarization only occurs when the material is stressed. As a result, the polarization is also short-lived. The difference, however, is that the silk films can be cycled repeatedly to regenerate the same signal. The stability of the signal given the same applied stress is seen in **Figure 30** and is stable for more than 130, 000 cycles, which corresponds to weeks of continuous, low frequency cycling. A material that can sustain its functionality for several weeks could be useful in biomedical applications.

As a functional biomaterial, piezoelectric silk could be used in a variety of different applications. First, as mentioned in the introduction, electric fields have been applied to cells to modulate cell response (Lorich *et al.*, 1998; Chang *et al.*, 2004; Brighton and McCluskey, 1988; Hartig *et al.* 2000). These studies have relied on traditional circuits that are bulky, rigid, and non-biocompatible. With piezoelectric silk's

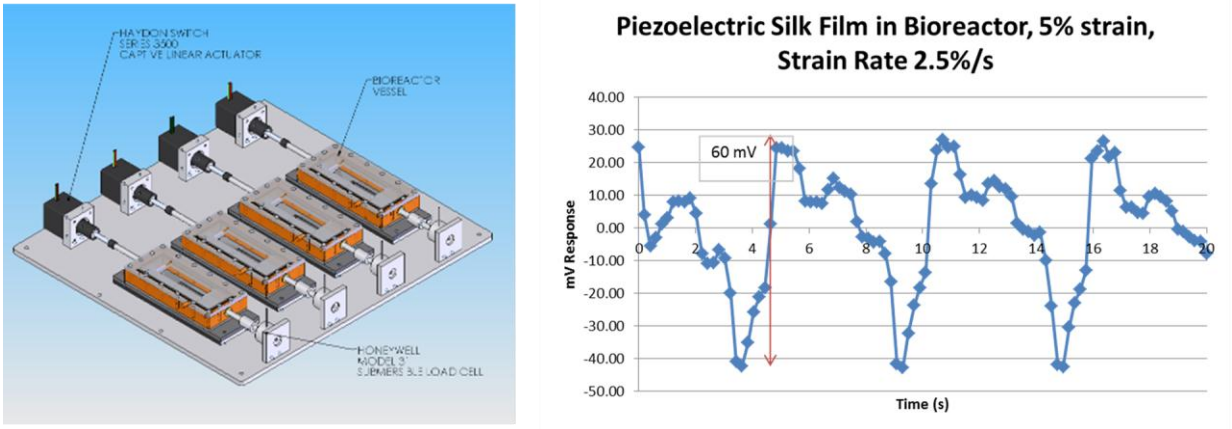

Figure 33: *Left:* Bioreactor designed by Kluge *et al.* (2010). *Right*: Piezoelectric silk film cycled in the bioreactor at 5% strain in air.

stable film lifetime and electric field generation in liquid, the films could be used in place of external circuitry typically used in studies. As an example, the bioreactor developed by Kluge *et al.* is capable of applying cyclic tensile and compressive strain on films for *in vitro* studies. Initial examination of piezoelectric film response in the bioreactor demonstrated that the films are capable of producing a measureable response in the bioreactor (**Figure 32**). Cycling films with cells cultured on the surface

would provide insight into the effect of silk's electric field on cell growth and differentiation *in vitro*, and its potential use as a functional biomaterial for tissue engineering.

Although the piezoelectric silk would not be a reliable quantitative sensor platform, it could be useful as a short-term monitor. For example, piezoelectric silk films could be used as digital sensors to determine when a threshold value has been reached, such as a maximum allowable strain. This would take advantage of the direct piezoelectric effect; below the cutoff point, the film is not stressed enough to produce a measurable voltage. Above the maximum allowable strain, however, a large voltage response would occur, which could be used as a notification that the threshold has been crossed. In another potential application, a minimum threshold can be determined, which would take advantage of the inverse piezoelectric effect. If a resonant frequency can be determined, piezoelectric silk films can be stimulated with an AC voltage that will lead to a maximum vibration, which in turn produces a resulting voltage. The produced voltage could be used as the basis for monitoring; as long as the voltage output remains above the threshold no action is necessary; as soon as it drops below the set value, however, a response is required. The output voltage is dependent on the extent of vibration, and the vibrations are influenced by the film's environment; in particular, mass on the surface will damp the vibrations and consequently reduce the output voltage. A rudimentary but real-time biosensor could be developed on this principle.

To make piezoelectric silk useful in a broader range of applications, it will be necessary to improve the piezoelectric effect in the material. If a large current or voltage value is required, changing the dimensions of the film can be used to increase the measured output for the desired application, as indicated by **Equations 17** and **21** and rewritten here:

$$d_{14} = \left(\frac{I_0}{A_E}\right) / \left(\frac{F_0}{A_{XS}}\right) \tag{17}$$

$$g_{14} = \left(\frac{V_0}{T}\right) / \left(\frac{F_0}{A_{XS}}\right) \quad (21)$$

Improving the draw ratio should also improve the piezoelectric effect as well; by improving the zone-drawing process to apply a specific stress to the film rather than force, it may be possible to reach higher draw ratios without breaking the film. Also, tightly regulating the film casting conditions to find the optimal initial secondary structures present in the film may help to reach a higher final draw ratio. It is known that relative humidity will influence the drying process, and films with increased β-sheet content do not draw well. Creating a controlled environment for film drying and determining the optimal conditions for the best zone-drawn films may lead to improved piezoelectric qualities. Finally, controlling polymer length—here silk fibroin fragments—may lead to improved zone-drawing by improving film uniformity for the zone-drawing process. By altering the degumming time, the average molecular weight of the silk fibroin will change. It may also be possible to filter out sizes that adversely affect the drawing process. Since the extent of alignment that occurs under the applied force is affected by how easily the silk can move within the glassy film during zone-drawing, more freely moving silk fragments will align more readily than bulky, tangled polymer chains.

Commercially produced PVDF is both zone-drawn and poled, and this combination may be beneficial to silk (Fukada, 1974). A PVDF film stretched to a draw ratio of 5 and then poled with a 300 kV/cm electric field led to a d_{14} constant of 30 pC/N and g_{14} constant of 350 mVm/N. By aligning the β-sheets and increasing β-sheet content through the zone-drawing process, the films will exhibit piezoelectricity as seen here. Zone-drawn films may be additionally subjected to a large electric field to align the dipoles and further improve the piezoelectricity, although it may only be a short-term effect based on the collagen electret work.

Lastly, water-annealed films were cured without any externally applied force. Previous work has shown that water immersion and stretching rather than zone-drawing can also induce alignment and

piezoelectricity, so water-annealing films under tension may further improve the alignment that would lead to increased piezoelectricity (Yucel *et al.*, 2011).

Future Directions

In addition to the application of piezoelectric pure silk films to biomedical applications, modified silk properties can be investigated as well. With an understanding of the structural components necessary to create the piezoelectric effect, modified materials could be created by conserving those structural components necessary for the effect while adding new material properties.

Preliminary studies adding glycerol to silk to create silk blends led to flexible films (**Figure 33**). The resulting films displayed piezoelectricity, and the addition of glycerol to increase flexibility could be useful for targeted applications (Lu *et al.*, 2010). The WAXS and FTIR results clearly show the alignment and β-sheet content present in pure silk piezoelectric films. The β-sheet content shifted from 28% in as-cast films to over 56% for a draw ratio of 3. DMA analysis of the films shows a markedly improved piezoelectric response of the films, with the largest d_{14} value of 2.9 pC/N. The effect in the glycerol blend films is one order of magnitude large than the effect seen in pure silk films. Optimizing the blend ratio may further improve the piezoelectric effect. At the same time, the different ratios will make the films more silk-like (less glycerol content) or more glycerol-like (less silk content) which again allows for tailored mechanical properties to match the application requirements.

More than merely creating blends of materials, new proteins can be designed for improved functionality. Recombinant proteins have highly uniform products and it is possible to control the protein product down to the specific amino acid sequence—attributes not found in native protein sources (Spiess *et al.*, 2010). Recombinant spider silks have been created based on dragline silks from *Navila clavipes* (Eisoldt *et al.*, 2011). Spider silks have long been known for their remarkable toughness,

and films made of these materials could be useful for applications where *B. mori* films' mechanical propertes are inadequate (Eisoldt *et al.*, 2011).

Here, recombinant spider silk protein C_{16} was used, which is based on *Araneus diadematus* dragline silk ADF-4 and is a 16-mer of module C shown in **Figure 34**. A 5 % (w/v) solution of C16 in HFIP was cast at 4°C to prevent aggregation and bubbles in the films. These films were then zone-drawn to draw ratios from 1.2 to 4, and analyzed using the DMA. The piezoelectric effect could be observed in films made of these much shorter, uniform proteins (**Figure 35**). FTIR analysis of films showed a similar peak shift toward the β-sheet region as is seen with *B. mori* silk films, shifting from 26% in as-cast films to 47% with a draw ratio of 4.4. Similarly, WAXS data show a weak appearance of the 020/002 plane that is visible in *B. mori* films, and also found in aligned native spider silk fibers (Riekel *et al.*, 1999). With proof that the piezoelectric effect can be recreated in films of recombinant silk, new proteins can be designed and produced to have more functionality, which could lead to an entirely new class of materials with multiple functionality tuned specifically to the desired application.

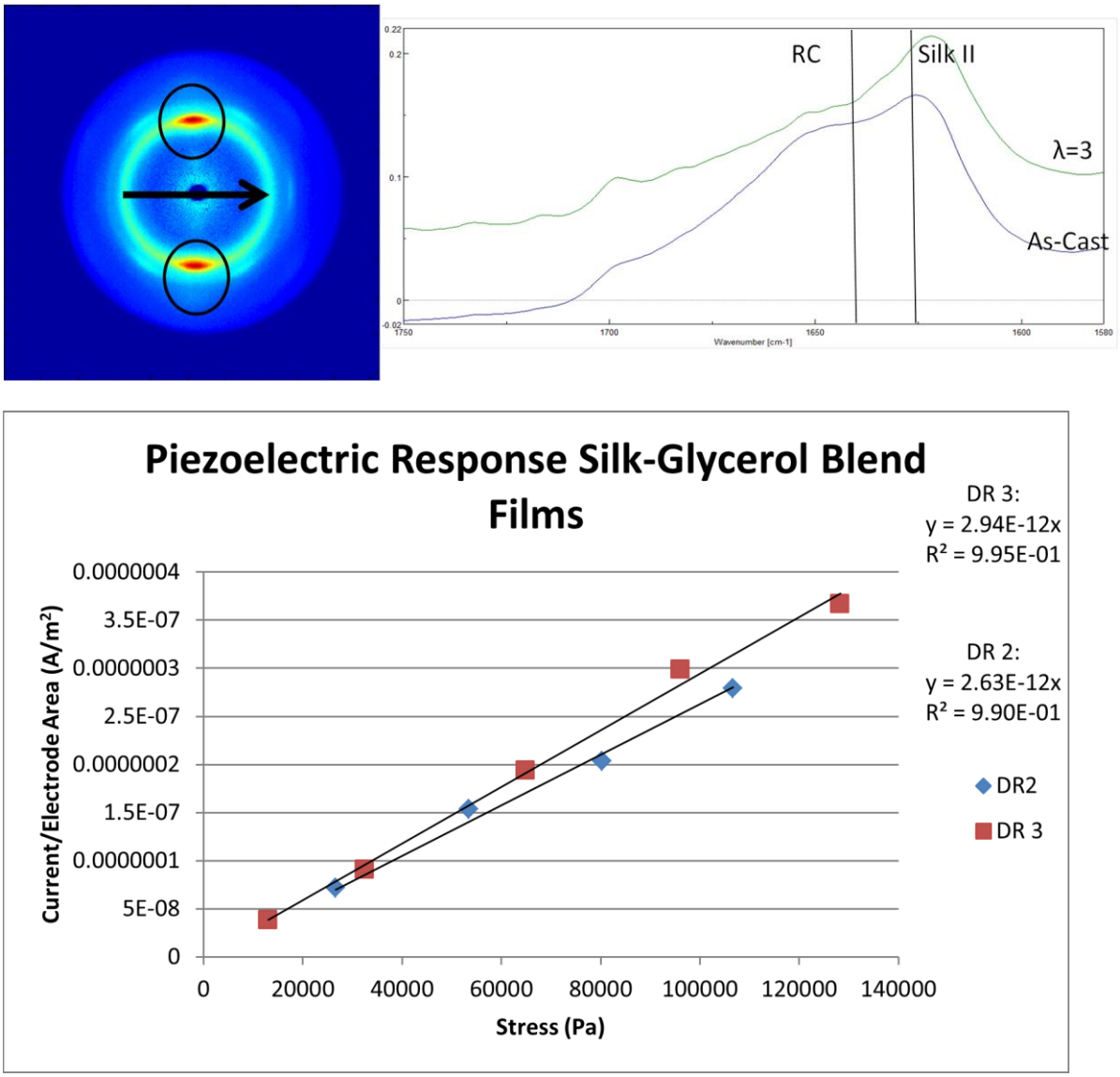

Figure 34: *Top Left:* WAXS results film s silk-glycerol blend film. Direction of alignment is horizontal, as indicated by the arrow. The strong appearance of the 020/002 plane indicates a highly oriented sample. Image courtesy of Dr. Peggy Cebe. *Top Right*: FTIR spectra of amide I band before and after zone-drawing. The drastic shift in amide I peak towards the β-sheet region indicates the zone-drawing process greatly increased the β-sheet content in the film, which is responsible for the piezoelectric effect. *Bottom:* Piezoelectric response of silk-glycerol film with increasing draw ratio (DR). As plotted here, the slope of the graphs is the d_{14} constant in C/N. The d_{14} of the films are 2.6 and 2.9 pC/N for a draw ratio of 2 and 3, respectively.

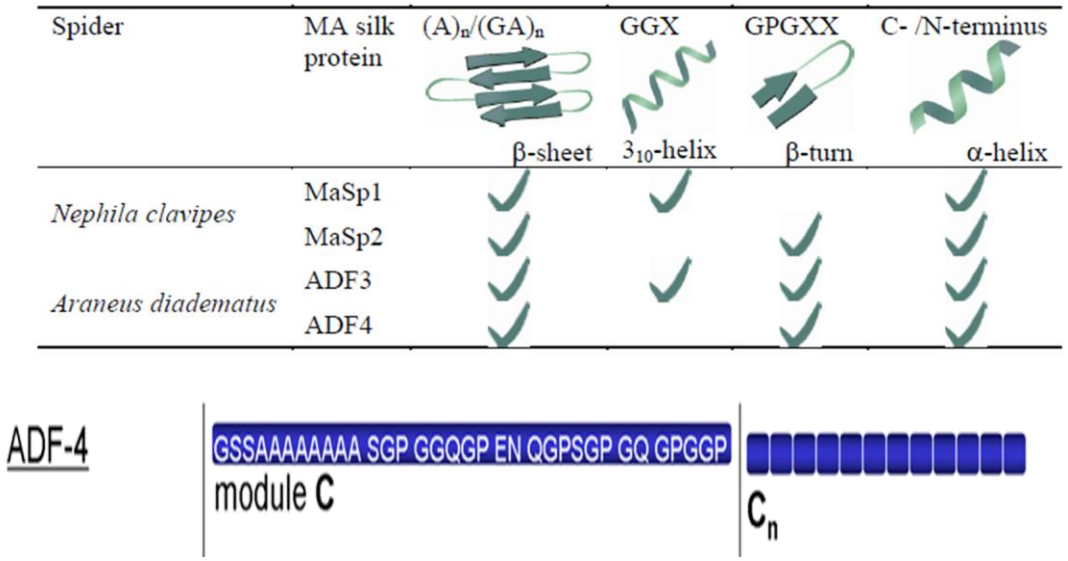

Figure 35: Recombinant spider silk proteins. *Top:* Chart summarizing the major secondary structures present in different major ampullate (MA) silks of two different species of spider (Humenik *et al.*, 2011). *Bottom:* The sequence of recombinant spider protein C_{16}, which is based on the repetitive sequence of ADF-4, a dragline silk of *A. diadematus*. The C_{16} protein consists of 16 repeats of the the C module (image courtesy T. Scheibel, University of Bayreuth).

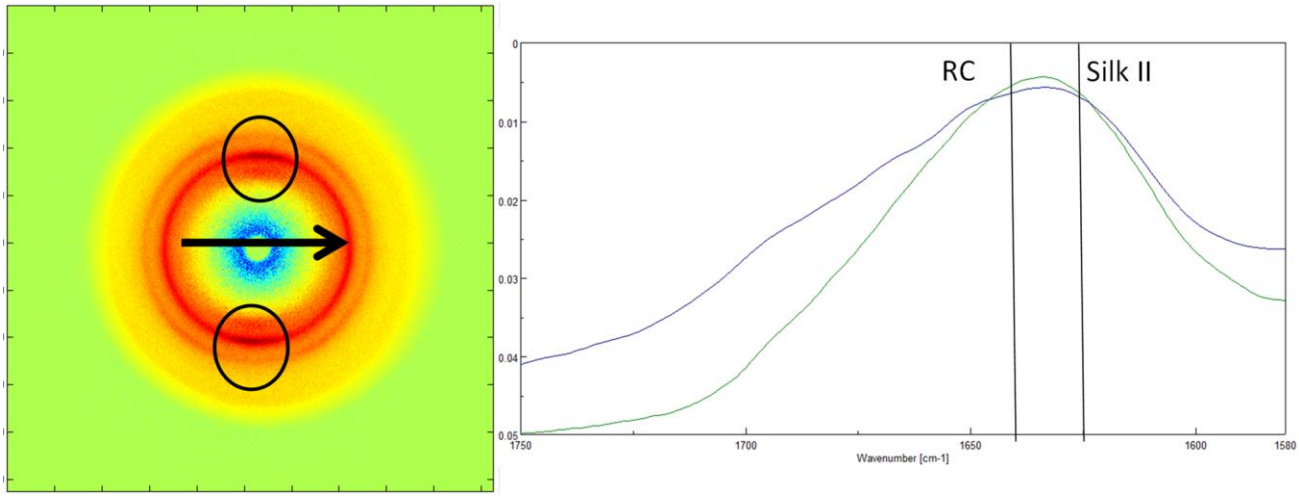

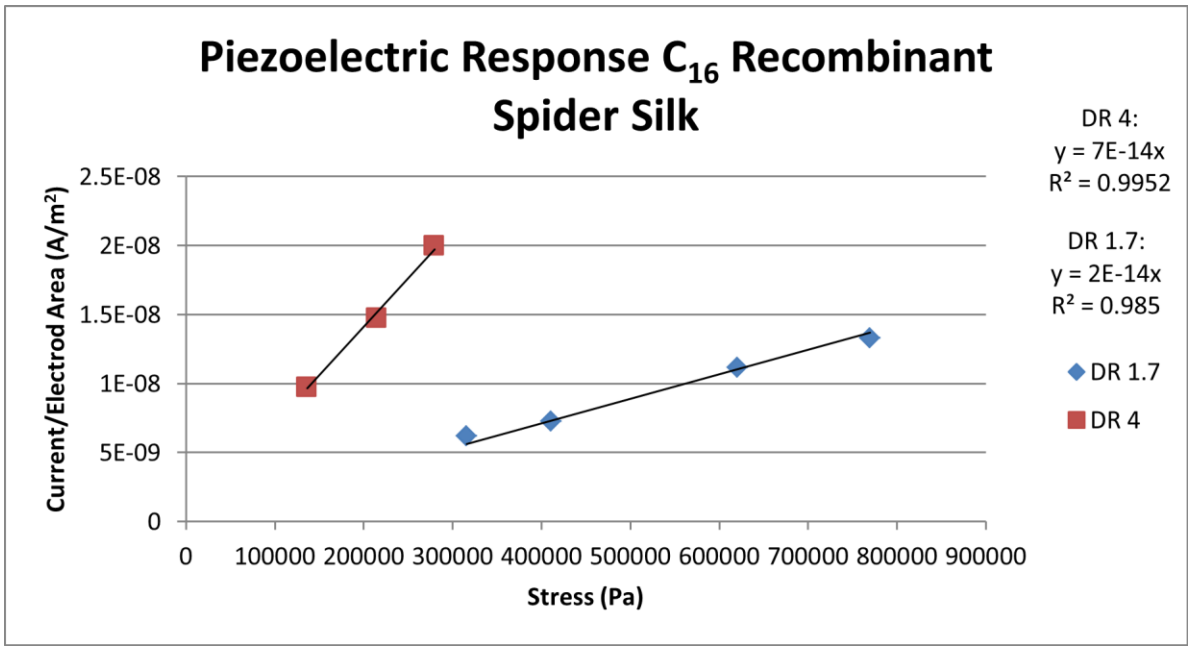

Figure 36: *Top Left:* WAXS results C_{16} protein in HFIP with a draw ratio of 2.6. Direction of alignment is horizontal, as indicated by the arrow. Weak bands circled indicate some alignment has occurred. Films of recombinant protein are very thin and the strength of the observed 020/002 plane may be limited by the amount of sample interrogated. Image courtesy of Dr. Peggy Cebe. *Top Right*: FTIR spectra of amide I band before and after zone-drawing. *Bottom:* Piezoelectric response of C_{16} protein in HFIP film with increasing draw ratio. As plotted here, the slope of the graphs is the d_{14} constant in C/N. The d_{14} of the films are 0.02 and 0.07 pC/N for a draw ratio of 1.7 and 4, respectively.

Works Cited

Altman GH, Diaz F, Jakuba C, Calabro T, Horan RL, Chen J, Lu H, Richmond J, Kaplan DL. Silk-based biomaterials. Biomaterials, 2003; 24: 401-416.

Anton SR, Sodano HA. A review of power harvesting using piezoelectric materials (2003-2006). Smart Materials and Structures, 2007; 16: R1-R21.

Atkinson GM, Pearson RE, Ounaies Z, Park C, Harrison JS, Dogan S, Midkiff JA. Novel piezoelectric polyimide MEMs. Transducers, Solid-State Sensors, Actuators and Microsystems, 12th International Conference, 2003; 1: 782-785.

Bassett CAL. Electrical effects in bone. Scientific American, 1965; 4: 18-25.

Brighton CT and McCluskey WP. Response of cultured bone cells to a capacitively coupled electric field: inhibition of cAMP response to parathyroid hormone. Journal Orthopoaedic Research, 1988; 6 : 567-571.

Brighton CT, Wang W, Seldes R, Zhang G, Pollack S. Signal transduction in electrically stimulated bone cells. Journal of Bone and Joint Surgery, 2001; 83A:1514-1523.

Bu N, Ueno N, Fukada, O. Monitoring of respiration and heartbeat during sleep using a flexible film sensor and empiricial mode decomposition. Proceedings of the 29th Annual International Conference onf the IEEE EMBS, 2007: 1362-1366.

Change W H-S, Chen L-T, Sun J-S, Lin F-H. Effect of pulse-burst electromagnetic field stimulation on osteoblast cell activities. Bioelectromagnetics, 2004; 25: 457-465.

Discher DE, Janmey P, Wang Y. Tissue cells feel and respond to the stiffness of their substrate. Science, 2005; 310: 1139-1143.

Eisoldt L, Smith A, Scheibel T. Decoding the secrets of spider silk. Materials Today, 2011; 14: 80-86.

Fukada E and Takashita S. Piezoelectric constant in β-form polypeptides, 1971; 10: 722-726.

Fukada E. Piezoelectric effects in collagen. Japanese Journal of Applied Physics, 1964; 3: 117-121.

Fukada E. Piezoelectric properties of biological polymers. Quarterly Review of Biophysics, 1983; 16:59-87.

Fukada E. Piezoelectric properties of organic polymers. Annals of New York Acadamy of Sciences, 1974; 238: 7-25.

Fukada E. Piezoelectricity of biopolymers. Biorheology, 1995; 32:593-609.

Furukawa T. Piezoelectricity and pyroelectricity in polymers. IEEE transactions on Electrical Insulation, 1989; 24:375-394.

Glynne-Jones P, Beeby S, White N. A method to determine the ageing rate of thick-film PZT layers. Measurement Science and Technology, 2001; 12: 663-670.

Gunatillake PA, Adhikari R. Biodegradable synthetic polymers for tissue engineering. European Cells and Materials, 2003; 5: 1-16.

Hartig M, Joos U, Wiesmann, H-P. Capacitively coupled electric fields accelerate proliferation of osteoblast-like primary cells and increase bone extracellular matrix formation in vitro. European Biophysics Journal, 2000; 29: 499-506.

Hayakawa R. and Wada Y. Piezoelectricity and related properties of polymer films. 1972; 1-55. **FIX**

Hronik-Tupaj M, Rice WL, Cronin-Golomb M, Kaplan DL, Georgakoudi. Osteoblastic differentiation and stress response of human mesenchymal stem cells. Biomedical Engineering Online 2011; 10:9.

Hu X, Kaplan, D, Cebe P. Determining beta-sheet crystallinity in fibrous proteins by thermal analysis and infrared spectroscopy. Macromolecules, 2006; 39: 6161-6170.

Hu X, Shmelev K, Sun L, Gil E-S, Park S-H, Cebe P, Kaplan DL. Regulation of silk material structure by temperature-controlled water vapor annealing. Biomacromolecules, 2011; 12: 1686-1696.

Huemmerich D, Helsen CW, Quedzuweit S, Oschmann J, Rudoph R, Scheibel T. Primary structure elements of spider dragline silks and their contribution to protein solubility. Biochemistry, 2004; 43: 13604-13612.

Humenik M, Smith AM, Scheibel T. Recombinant spider silks—biopolymers with potential for future applications. Polymers, 2011; 3: 640-661.

Jaffe H. Piezoelectic ceramics. Journal of the American Ceramic Society, 1958; 41: 494-498.

Kaplan D, Adams WW, Farmer B, Viney C. Silk: biology, structure, properties, and genetics. Silk Polymers. American Chemical Society, 1994. Pp 2-16.

Kepler RG and Anderson RA. Pieozelectricity in polymers. Critical Reviews in Solid State and Materials Sciences, 1980; 9: 399-447.

Kluge JA, Leisk GG, Cardwell RD, Fernandes AP, House M, Ward A, Dorfmann AL, Kaplan DL. Bioreactor system using noninvasive imaging and mechanical stretch for biomaterial screening. Annals of Biomedical Engineering, 2011; 39:1390-1402.

Levin M. Bioelectric mechanisms in regeneration: unique aspects and future perspectives. Seminars in Cell and Developmental Biology, 2009; 20:543-556.

Lewis PR, Manginell RP, Adkins DR, Kottenstette RJ, Wheeler DR, Sokolowski SS, Trudell DE, Byrnes JE, Okandan M, Bauer JM, Manley RG, Frye-Mason GC. Recent advancements in the gas-phase MicroChemLab. IEEE Sensors Journal, 2006; 6: 784-795.

Lorich DG, Brighton CT, Gupta R, Corsetti JR, Levince SE, Gelb ID, Seldes R, Pollack SR. Biochemical pathway mediating the response of bone to capactive coupling, 1998; 350: 246-256.

Lotz B, and Cesari FC. The chemical structure and crystalline structures of *Bombyx mori* silk fibroin. Biochimie, 1979; 61: 205-214.

Lu S, Wang X, Lu Q, Zhang X, Kluge JA, Uppal N, Omenetto F, Kaplan DL. Insoluble and flexible silk films containing glycerol. Biomacromolecules, 2010; 11: 143-150.

Marino AA, Spadaro JA, Fukada E, Kahn LD, Becker RO. Piezoelectricity in collagen films. Calcified Tissue International, 1980; 31: 257-259.

Marsh RE, Corey RB, Pauling L. An investigation of the structure of silk fibroin. Biochimica et Biophysica Acta, 1955; 16: 1-34.

Martin RM. Piezoelectricity. Physical Review B, 1972, 5: 1607-1613.

Marx KA. Quartz crystal microbalance: a usefule tool for studying thin polymer films and complex biomolecular systems at the solution-solvent interface. Biomacromolecules, 2003; 4: 1099-1120.

Mascarenhas S. Bioelectrets: electrets in biomaterials and biopolymers. Topics in Applied Physics, 1987; 33: 321-346.

McCaig CD, Rajnicek AM, Song B, Zhao M. Controlling cell behavior electrically; current views and future potential. Physiology Review, 2005; 85:943-978.

Numata K, Cebe P, Kaplan DL. Mechanism of enzymatic degradation of beta-sheet crystals. Biomaterials, 2010; 31: 2926-2933.

Ounaies Z, Young J, Harrison J. An overview of the piezoelectric phenomenon in amorphous polymers. Field Responsive Polymers, 1999; 88-103.

Riekel C, Braenden, Craig C, Ferrero C, Heidelbach F, Mueller M. Aspects of X-ray diffraction on single spider fibers. International Journal of Biological Macromolecules, 1999; 24: 179-186.

Rockwood DN, Preda RC, Yucel T, Wang X, Lovett ML, Kaplan DL. Materials fabrication from *Bombyx mori* silk fibroin. Nature Protocols, 2011; 6: 1612-1631.

Shen Y, Johnson MA, Martin DC. Microstructural characterization of *Bombyx mori* silk fibers. Macromolecules, 1998; 31: 8857-8864.

Shimono T, Matsunaga S, Fukada E, Hattori T, Shikinami Y. The effects of piezoelectric poly-l-lactic acid films in promoting ossification *in vivo*, 1996; 10: 471-476.

Silva CC, Thomazini D, Pinheiro AG, Aranha N, Figueiro SD,Goes JC, Sombra ASB. Collagen-hydroxyapatite films: piezoelectric properties. Materials Science and Engineering, 2001; B86: 210-218.

Sirohi J, Chopra I. Fundamental understanding of piezoelectric strain sensors. Journal of Intelligent Material Systems and Structures, 2000; 11: 246-257.

Spiess K, Lammel A, Scheibel T. Recombinant spider silk proteins for applications in biomaterials. Macromolecular Bioscience, 2010; 10: 998-1007.

Sun S, Kou T, Zhu H. A study on bioelectret collagen. Journal of Applied Polymer Science, 1996; 64: 267-271.

Sundelacruz S, Levin M, Kaplan DL. Membrane potential controls adipogenic and osteogenic differentiation of mesenchymal stem cells, 2008; 3:e3737.

Sundelacruz S, Levin M, Kaplan DL. Role of membrane potential in the regulation of cell proliferation and differentiation. Stem Cell Rev and Rep, 2009; 5:231-246.

The piezoelectric effect. Tech-FAQ, 2012. Accessed 25 May 2012. <http://www.topbits.com/piezoelectric-effect.html>
Horan RL, Antle K, Collete AL, Wang Y, Huang J, Moreau JE, Volloch V, Kaplan DL, Altman GH. In vitro degradation of silk fibroin. Biomaterials, 2005; 26: 3385-3393.

Tucker J. Optimizing low-current measurements and instruments. Keithley Instruments, Inc White Paper. http://www.keithley.com/products/dcac/sensitive/highresistance/?path=6517B/Documents#9 accessed 23 May 2012.

Vendrely C, and Scheibel T. Biotechnological production of spider-silk proteins enables new applications. Macromolecular Bioscience, 2007; 7: 401-409.

Vepari C, Kaplan DL. Silk as a biomaterial. Progress in Polymer Science, 2007; 32: 991-1007.

Yang X, Gu J, Zhu H. Preparation of bioelectret collagen and its influence on cell culture *in vitro*. Journal of Materials Science: Materials in Medicine, 2006; 17:767-771.

Yang XL, Li BS, Gu JW, Sun S, Zhu HS. Influence of bioelectret collagen on cell growth in vitro. Proceedings of the 20th Annual International Conference of the IEEE Engineering in Medicine and Biology Society, 1998; 20: 2970-2973.

Yeung T, Georges PC, Flanagan LA, Marg B, Ortiz M, Funaki M, Zahir N, Ming W, Weaver V, Janmey P. Effects of substrate stiffness on cell morphology, cytoskeletal structure, and adhesion. Cell Motility and Cytoskeleton, 2005; 60: 24-34.

Yucel T, Cebe P, Kaplan DL. Structural origins of silk piezoelectricity, 2011; 21:779-785.